Somatosensory Cortical Processing In The Mouse Forepaw System

DISSERTATION

zur Erlangung des akademischen Grades

Doctor of Philosophy

Ph.D.

im Fach Biologie

eingereicht an der

Lebenswissenschaftliche Fakultät

der Humboldt-Universität zu Berlin

von

Master of Science

赵 文 杰

Zhao Wen-Jie

Präsidentin der Humboldt-Universität zu Berlin

Prof. Dr.-Ing. Dr. Sabine Kunst

Dekan der Lebenswissenschaftliche Fakultät

der Humboldt-Universität zu Berlin

Prof. Dr. Richard Lucius

Gutachter/innen:

Prof. Dr. Michael Brecht

Prof. Dr. Richard Kempter

Dr. James F. A. Poulet

Tag der mündlichen Prüfung:

08.09.2016

HELMHOLTZ ASSOCIATION

MDC MAX DELBRÜCK CENTER FOR MOLECULAR MEDICINE IN THE HELMHOLTZ ASSOCIATION

HUMBOLDT-UNIVERSITÄT ZU BERLIN

Somatosensory Cortical Processing In The Mouse Forepaw System

PhD candidate:

赵 文 杰

Zhao Wen-Jie

Supervisor：

Dr. James. F. A. Poulet　Prof. Dr. Michael Brecht

Table of Contents

Abstract

The primary somatosensory cortex (SI) is composed of six layers (L1-L6). The coordination of neural activities across six layers of cortical neurons is essential for reliable sensory perception and the control of voluntary behavior. However, the synaptic neural mechanisms governing translaminar cortical processing in behaving animals are still unknown. I made in vivo single and dual whole-cell recordings in mouse forepaw SI, my work revealed that L2/3 and L5 pyramidal neurons have distinct intrinsic properties and membrane potential dynamics during forepaw behavior. Dual recordings showed that sensory- and movement-evoked synaptic inputs were closely correlated across layers, but low frequency subthreshold fluctuations and spontaneous action potentials exhibited a laminar specific temporal profile. At longer time scales, my data showed that spontaneous forepaw movement evoked a de-correlation of subthreshold activity across layers. Furthermore, L5 pyramidal neurons signaled sensory-evoked and spontaneous forepaw movements more strangely than L2/3 neurons. Overall, my work suggests that laminar differences in the timing of action potential firing, subthreshold synchrony and mean firing rates are dependent both on the origin of the underlying synaptic input and the behavioral outcome of the event. In addition, I identified that forepaw SI neurons respond to mild cooling stimulation of the forepaw and that this response is mediated by the Transient receptor potential cation channel subfamily M member 8 (TRPM8) in primary sensory afferent neurons.

Zusammenfassung

Der primäre somatosensorische Kortex (S1) besteht aus sechs Schichten (L1-L6). Die koordinierte Aktivität dieser sechs Schichten kortikaler Neurone ist entscheidend für die sensorische Wahrnehmung und die Steuerung willkürlichen Verhaltens. Es ist jedoch noch wenig über die synaptischen Mechanismen bekannt, die die Verarbeitung zwischen den kortikalen Schichten bei sich aktiv verhaltenden Tieren bestimmen. Ich habe einfache und doppelte in vivo-Ganzzellableitungen im Vorderpfoten-Areal von S1 in der Maus gemacht, und gezeigt, dass Pyramidalzellen in L2/3 und L5 während einer Bewegung der Vorderpfote Unterschiede in ihren intrinsischen Eigenschaften und der Dynamik ihrer Membranpotenziale zeigen. Doppelableitungen haben gezeigt, dass sensorisch und motorisch ausgelöste synaptische Eingänge zwischen den Zellschichten weitgehend korreliert waren, niederfrequente unterschwellige Potenzialschwankungen und spontane Aktionspotenziale jedoch einen schichtspezifischen Zeitverlauf zeigten. Auf einer längeren Zeitskala beobachteten wir, dass spontane Bewegungen der Vorderpfote eine Dekorrelation unterschwelliger Aktivität zwischen den Schichten auslösten. Des Weiteren zeigten L5-Pyramidalzellen durch ihre Aktivität sensorisch ausgelöste und spontane Bewegungen der Vorderpfote stärker an, als L2/3-Neurone. Insgesamt deuten meine Daten darauf hin, dass Unterschiede zwischen den Zellschichten beim Timing von Aktionspotenzialen, bei der unterschwelligen Synchronisierung und bei den mittleren Feuerraten sowohl von der Quelle des zu Grunde liegenden synaptischen Eingangs als auch vom resultierenden Verhalten abhängen. Außerdem konnte ich zeigen, dass Neurone im Vorderpfoten-Areal von S1 auf leichte Kältereizung der Vorderpfote antworten, und dass diese Antwort vom

Ionenkanal transient receptor potential cation channel subfamily M member 8 (TRPM8) in primären sensorischen afferenten Neuronen vermittelt wird.

1. INTRODUCTION

A central issue in neuroscience is to decipher the relationship between sensory perception and behavior and the activity of neurons embedded in synaptically connected networks. A main neural structure in the brain which is directly involved in sensory perception, cognition and voluntary movement control is the cerebral cortex. A particular feature of cortical circuit structure is its arrangement into 6 layers (except for agranular cortex) that have distinct functions. Understanding how the layers work together is difficult given that each layer contains many cell types synaptically connected into complex microcircuits. Moreover, relating the activity and function of these neurons requires examination *in vivo* in behaving animals.

The level of synchrony of neural activity across layers is believed to be an important aspect of cortical functions. Extracellular recordings of cortical neurons across layers have shown distinct patterns of synchrony during sensory processing and spontaneous activity (Sakata & Harris, 2009). Synchronous action potential firing is generated by synchronous synaptic input to cortical neurons. Subthreshold membrane potential synchrony has never been examined across cortical layers in awake mice. In my thesis I aim to investigate synaptic mechanisms of translaminar synchrony in primary somatosensory cortex. The synaptic mechanisms of translaminar processing can best be studied in a cortical region that is easy to access in an awake animal engaged in behavior. I chose to study the primary sensory cortex of the mouse forepaw system which is amendable to these needs.

1.1 The mouse forepaw somatosensory system – from sensory afferents to thalamus

Mice use their forepaws for complex manipulations and the active sensing of a wide range of objects. The forepaw bear a structural resemblance to hands in primates, but the thumb is retrograde to a digit bud (Figure 1). At the periphery, touching and cooling to the glabrous skin of the forepaw is transduced into electrical action potentials by a wide variety of both myelinated and unmelyinated sensory afferent, which are Aα, Aβ, Aδ and C fibers (Vallbo & Johansson, 1984; Johnson, 2001). These neurons synapse in the dorsal horn of the spinal cord and ascend to the cuneate nucleus (CN) (for touch), while for temperature the pathway is less well understood.

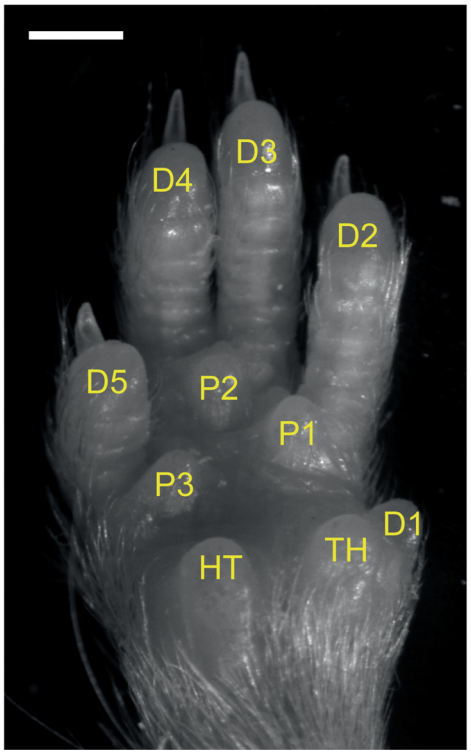

Figure 1. A mouse forepaw
An image of mouse right forepaw at glabrous side show morphology of digits(D1-D5) and pads(central pads:P1-P3; TH–thenar pad and HT–hypothenar pad).
Scale bar: 1mm

Ascending sensory projections from the CN travel across the midline of the brain stem (Figure 2). The sensory information carried by these ascending neurons is relayed to ventral posterior lateral nucleus (VPL) within the thalamus, which also forward information of sensory projections from the hind-limbs and trunk.

The thalamus consists of a complex of several nuclei which are responsible for relaying primary sensory signals to the neocortex. Some of these nuclei receive primary sensory information from specific sensory areas (such as the paw, face and trunk, etc.), then transmit it to specific cortical regions with targeted axonal projections in the cortex. For example, in the mouse thalamus, the VPL relays to the forepaw and hindpaw regions of

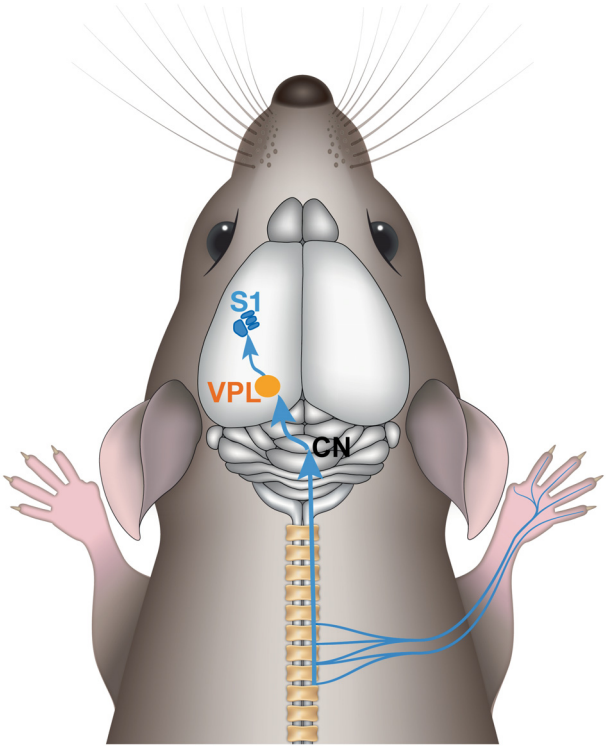

Figure 2. Somatosensory pathway in mouse forepaw system. Peripheral sensory fibers underlying forepaw glabrous skin with expression of mechano- and thermal-receptors relay along spinal cord through dorsal root ganglia, then terminated in cuneate nuclei (CN) in brain stem, neurons in CN convey to the contralateral ventro-posterior lateral (VPL) nuclei in thalamus, where primary sensory signals ascend to primary somatosensory cortex (SI).

primary somatosensory cortex (SI), and the ventral posterior medial nucleus (VPM) relays to whisker region of SI. Another set of higher order nuclei, for example the posterior medial nucleus (POm), are driven strongly by cortical feedback projections and have broad axonal arbors in the cortex(Deschênes et al., 1998; Wimmer et al., 2010; Mease et al., 2016). In addition to their function as relays of sensory signals, these thalamic nuclei also modulate signal strength in a way which is correlated with and modulates cortical states (Poulet et al., 2012).

1.2 Primary somatosensory cortex - anatomy

Ventral posterior thalamic nuclei projections exclusively target the mammalian SI. While less is known about the forepaw thalamocortical pathway projection, the thalamocortical microcircuits involved in the SI whisker barrels region have been extensively investigated and mapped and are thought to resemble the structure in forepaw cortex (Meyer et al., 2010a; Feldmeyer, 2012; Feldmeyer et al., 2013; Jouhanneau et al., 2014). Thalamic projections to SI are distributed in a layer-specific manner, as seen in a simplified model in Figure 3. Projections from the corresponding VPM (for whisker input) and VPL (for forepaw input) predominantly target layer 6 (L6) and layer 5 (L5B), and barrel fields in the granular layers (L4), ending in layer 3 (L3) (Chmielowska et al., 1989). Projections from the POm terminate predominantly in cortical L5a and to layer 1(L1) (Wimmer et al., 2010a; Ohno et al., 2012). Evidence has accumulated from a number of studies to indicate that L4 is the major target of the thalamus, and the main source of sensory input to L2/3. However recent work has shown direct input to L5

(Constantinople & Bruno, 2013). L2/3 neurons communicate with each other and project to other cortical regions. L5 houses output neurons that project subcortically (de Kock and Sakmann, 2009; Meyer et al.,2010b). Its projection relays information to subcortical-regions (the striatum, brain stem, midbrain, and spinal cord) (Wise & Jones, 1977; Hattox & Nelson, 2007;

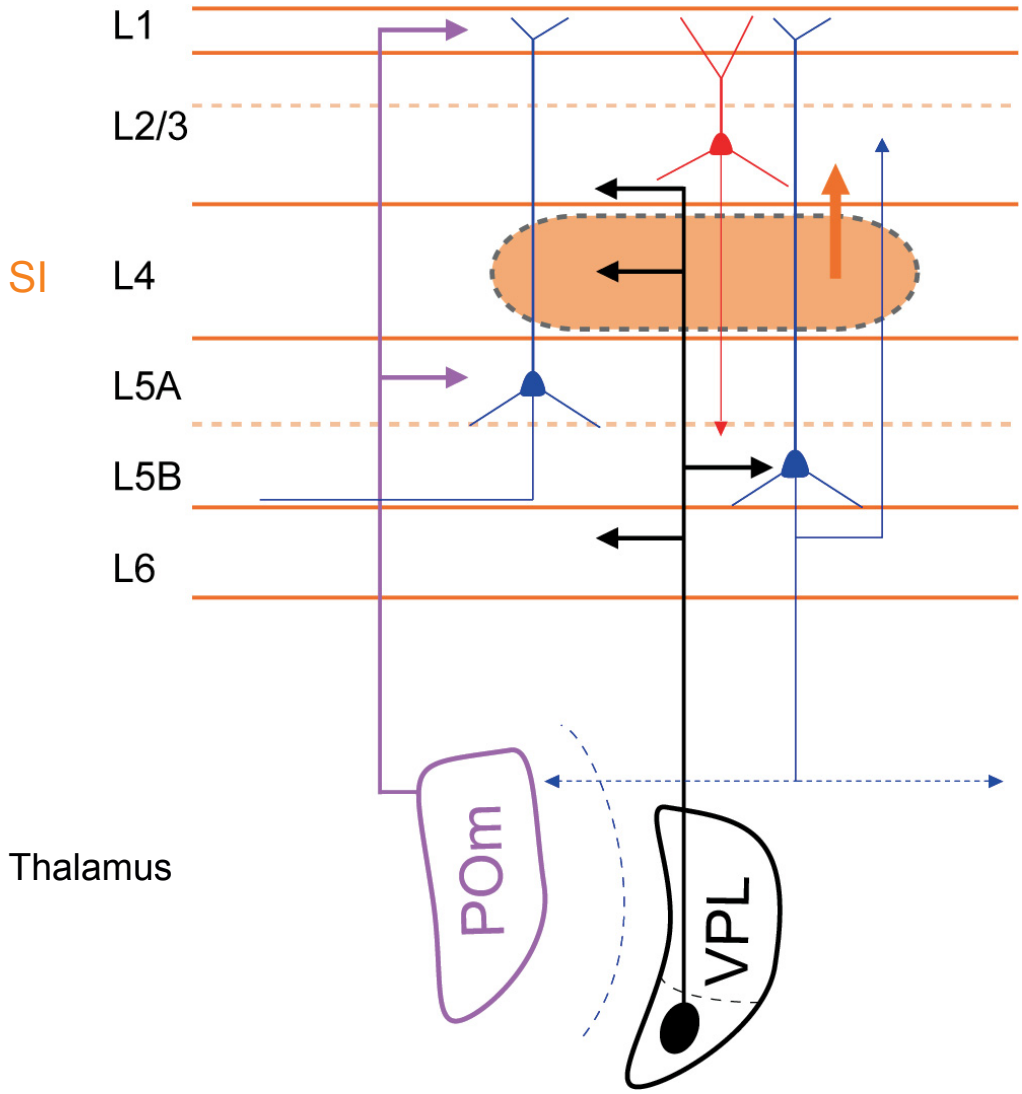

Figure 3. Schematic of simplified thalamocortical and tanslaminar cortical circuits for SI forepaw.
Thalamocortical tactile sensory circuits and tanslaminar between L2/3 and L5 cortical circuit in SI, excitatory sensory inputs from thalamus ventral posterior lateral (VPL) and posteromedial (POm) nuclei project to SI. VPL projects to L6 and L5B, L4(barrel region, in orange), and L3, whereas POm projects to L5A, L1 and L2. Thick solid lines show projections from thalamus to SI, thicker orange line show projection from L4 to L2/3, thin solid lines show circuits in SI, dash lines show circuits leaving SI.

Groh et al.,2010; Pidoux et al., 2011) and the contralateral hemisphere (Hattox & Nelson, 2007).

The primary somatosensory cortex is arranged into columns of somatosensory maps. Since Vernon Mountcastle first illustrated that the neocortex is composed of functional columns or mini-columns of neurons (Mountcastle, 1957, 1997), this model has guided work on many different systems (Wiesel & Hubel, 1974; Mountcastle,1997), and is particularly suited for studies of somatosensory processing in rodents (Feldmeyer et al., 2013). The columns of the SI are arranged into a form termed the barrel cortex, which has large cortical regions devoted to sensory processing from specific parts of the body: the forepaw, hind-paw, trunk, whisker, and lower lip. In mice the "barrel" arrangement of the SI for whiskers is prominently seen in cytochrome oxidase staining of cortical layer 4 (L4) (Woolsey & Van der Loos, 1970). The topographical arrangement of barrels mirrors the arrangement of whiskers on the rodent's snout. The barrels in the forepaw SI are smaller in mice than rats (Cases et al., 1996**,** Pearson et al., 1999)**.** They do, however, form a basic column-like structure (Cases et al., 1996; Lee & Kim, 2012), as do all the other nerves of the SI.

The connectivity of primary SI neurons has received a great deal of attention in both *in vivo* and brain slice works which have mapped connections both between and within layers. Details of the underlying local and translaminar connectivity in whisker SI have been elucidated from cortical slice experiments (Feldmeyer, 2014). It has been shown that SI is a cortical region consisting of 6 distinct layers, composed mainly of 85%

excitatory and 15% inhibitory neurons. The exception is L1, which contains only inhibitory interneurons. Studies based on brain slices and anesthetized animals have shown that in L2/3 and L5, communication between excitatory and inhibitory neurons forms a strong, tight cortico-cortical network within and across cortical layers. In L2/3, interneurons are connected to pyramidal neurons and other types of interneurons, which form a feedforward inhibition and feedback disinhibition network (Petersen, 2014). Meanwhile, L2/3 interneurons also send inhibition to L4/5 which might act as a feedback to modulate excitatory inputs from these layers(Helmstaedter et al., 2009). In L5, there is a typical disynaptic feedforward inhibition from a neighbor pyramidal neuron, which is mediated by a interneuron in L5 – Martinotti interneuron (Silberberg & Markram, 2007; Murayama et al., 2009). Such disynaptic inhibition is shown to regulate frequency-dependent synaptic transmission and sensory coding(Murayama et al., 2009).

Layer 5 excitatory neurons (L5) act as the interface for cortico-cortical and -subcortical communication, as seen by the fact that they are the targets of massive excitatory inputs from the thalamus (Meyer, 2010a) and higher-order projections (Manita et al., 2015). Furthermore, the L5 delivers information that has been integrated in the SI to other cortices and the spinal cord via long-range connections. This creates a bridge between the neocortex and the rest of brain, strongly suggesting that L5 might be a center of cortical decision-making for signals induced by sensory perception (Houweling & Brecht, 2008). Therefore, it is demanded to investigate the synaptic properties and mechanism of cortical processing in L5.

So far, studies based on brain slices and anesthetized animals have shown that monosynaptic connections between excitatory neurons of the same layer at about 10% between pyramidal neurons and at much higher rates to inhibitory neurons, besides, connection rate are also dependent on the size of zone around a pyramidal neuron (Perin et al., 2011). Excitatory neurons in different layers are also connected at slightly lower rates. It revealed that a defining feature of the cortex is the sparse connected recurrent network (Lefort et al., 2009; Petreanu et al., 2009; Gentet et al., 2010; Adesnik & Scanziani, 2010; Hooks et al., 2011; Perin et al., 2011; Feldmeyer, 2012; Harris & Mrsic-Flogel, 2013; Xue et al., 2014). Several important questions still remain: How correlated is membrane potential activity across layers, and how does synaptic potential in different cortical layers relate to the behavior of an animal? To our knowledge, this question has yet to be investigated in animals that are awake.

1.3 Sensory processing of layer 2/3 and layer 5 excitatory neurons

Sensory coding in the SI barrel cortex has been shown to have layer-specific activity. In supragranular layers, many studies have shown that the sensory-evoked firing rate is quite low in pyramidal neurons, no matter whether animals are awake or anesthetized (Brecht et al., 2003; Crochet & Petersen, 2006; de Kock et al., 2007; O'Connor et al., 2010; Barth & Poulet, 2012). However, in granular and infragranular layers (Brecht et al., 2002; Manns et al., 2004), the rate of sensory-evoked firing is higher, and the thick tufted pyramidal neurons in L5 exhibit the highest sensory evoked firing rates of

recorded excitatory neurons. Overall, L2/3 is characterized as sparse-coding whereas L5 as dense-coding (Barth & Poulet, 2012). However, all of this data has focused on the sensory response properties of single cells, so it is still not clear whether sensory responses within individual cortical layers correlate with each other in response to the same stimulus, in the same temporal window, during different behavioral states.

1.4 Cortical States

The term “brain state” originated from studies of sleep. Electroencephalography (EEG) studies of the human cerebral cortex during slow-wave sleep revealed characteristically synchronized, slow oscillations dominated by a low frequency with large amplitude. In contrast, during wakefulness and/or rapid eye movement (REM) sleep, the cortex was quite active and exhibited a pattern dominated by fast fluctuations in frequency, with a slow frequency oscillation that was abolished and desynchronized overall (Jasper, 1941; Steriade et al., 2001, 2005).

Early EEG studies had revealed that changes in brain state were present on a large scale across many cortical neurons/regions. Could their characteristics be observed in intracellular membrane potential activity as well? Recent studies based on intracellular recordings made in awake animals indicate that brain states have a more complex profile. These works found low and high frequency oscillations interwoven in phasic patterns in the animals' cerebral cortex (Crochet & Petersen, 2006; Poulet & Petersen, 2008; Tan et al., 2014). The cortex of head-fixed awake but resting mice

exhibits a low frequency but highly synchronized activity which is characteristic of phases of quiet wakefulness. These slow (<5 Hz) fluctuations are shorter in duration and therefore the frequency is not as low as the patterns seen in anesthetized animals, or those in a state of slow-wave sleep. In behaving animals, the fluctuations in low frequencies are suppressed and replaced by fast-frequency oscillations (e.g., beta and gamma bands). In quiet phases, the membrane potential (V_m) correlates with background activity (local field potential, LFP) and in some cases, the distribution of membrane potential exhibits like a bimodality pattern. Once animals begin moving, the V_m correlates with the behavioural state. The bimodal distribution of V_m is lost, along with the widely varying fluctuations of amplitude. Whole-cell recordings from neighbouring excitatory neurons in L2/3 have also shown that slow large amplitude events are highly correlated but the active states results in a desynchronized membrane potential activity (Poulet & Petersen, 2008).

The slow oscillations seen in animals in a quiet, wakeful mode are more irregular (in terms of amplitude and frequency) than those observed in anesthetized animals (Crochet & Petersen, 2006; Poulet & Petersen, 2008; Chauvette et al., 2010; Tan et al., 2014). This suggests that cortical networks are highly dynamic when an animal is awake. Besides, data from extracellular recordings and intracellular recordings using sharp electrodes have shown slow oscillations in anesthetized brains, which start earlier, often in deep layers (Sakata & Harris, 2009; Chauvette et al., 2010). The same studies have shown that the firing rates in infra-granular layers are higher.

Are these really signatures of slow cortical fluctuations, or are they simply side effects of anesthesia? Furthermore, how synchronous are activities across cortical layers, and with respect to behavior state?

Resolving these questions will probably require making direct measurements of membrane potentials in different layers of the neocortex in animals that are awake. Previous data have mainly been obtained from L2/3, with the exception of a few recordings from deep layers in anesthetized (Chauvette et al., 2010) or paralyzed animals (Constantinople & Bruno, 2013).

1.5 State dependent sensory processing

Cortical neurons process sensory inputs in a state-dependent manner. Earlier EEG data had indicated interactions between the cortical state and sensory input (Adrian & Matthews, 1934). Previous reports based on intracellular recordings from anesthetized animals describe only how sensory input is processed at different membrane potential levels (Ferster & Jagadeesh, 1992). Then recent studies have shown a reduction in subthreshold amplitude and spiking responses in depolarized upstates in anesthetized animals (Petersen et al., 2003; Sachdev et al., 2004), but recordings from different cortical regions have also shown differences in state-dependent modulations (Haider et al., 2007), for instance, in cat primary visual cortex (VI), amplitude of evoked subthreshold activity did not enhance as much as evoked spikes during “up” state. Recently, *in vivo* recordings from different sensory cortices and the thalamus in awake animals have suggested that the

brain state influences sensory inputs in a complex pattern (Crochet & Petersen, 2006, Niell & Stryker, 2010, Bennett et al., 2013, Polack et al., 2013).

The cortical activity of animals that are awake is more dynamic, and the mechanisms that integrate sensory processing with states of behaviour seem to differ between cortical regions. In the mouse whisker system, brief whisker stimuli evoked a subthreshold and occasionally a spiking response in L2/3 neurons, the amplitude of subthreshold response is reduced during whisker movements as compared to the response in quiet resting mice (Crochet & Petersen, 2006). Interestingly the action potential firing rates remained the same. A similar finding was observed in auditory cortex of awake mice, for example, a tone stimulus delivered while an animal was moving caused a drop in the firing rates in L2/3 neurons, while firing activity in L4 and the thalamus remained unchanged. In contrast in the rodent VI, visual stimulation evoked higher firing rates in moving animals than in quiet ones (Niell & Stryker, 2010, Bennett et al., 2013, Polack et al., 2013), even in the absence of additional input from the thalamus.

Further studies have shown that modes of sensory processing in awake mice might also differ between cortical layers (Zhou et al., 2014). These data suggest that cortical sensory processing in awake animals is carried out in a modality- and layer-specific manner.

Such experiments have produced data from awake and anesthetized animals, but almost all of it has been obtained from the supra-granular layer (L2/3). Almost nothing is known about the dynamics of membrane potentials

in infra-granular layers during sensory processing in awake animals, the only studies in awake animals from deeper layers have pooled recordings across layers (McGinley et al., 2015). Measurements in L5 would be particularly interesting, given its role as the "output" layer of the cerebral cortex.

1.6 How to examine synaptic mechanisms of cortical synchrony *in vivo*

To understand how information is processed in the SI at the level of synaptic input, and how degrees of synchrony are modulated across layers, the neural activities of each component in SI need to be measured simultaneously in each layer. A number of techniques have been developed to investigate electrophysiological activity *in vivo*, each providing particular advantages in some contexts and limitations in others. Extracellular recordings could provide relative high temporal resolution and good stability but no information on the subthreshold synaptic activity within neurons. Sharp-electrode intracellular recordings allow membrane potential measurements (albeit with leaky current noises) but are not stable in awake animals. Imaging technology using voltage sensitive dye (VSD) (Gong et al., 2015) is promising, but still in its infancy and has not yet reached a stable precise resolution in supra granular layers in awake behaving animals, let alone neurons in deeper layers. To overcome these technical limitations, I used *in vivo* whole-cell patch-clamp recording. The giga-seal formed between the glass recording pipette and cell membrane provides recording stability even in awake animals (Margrie et al., 2002). Moreover at the end of recording, cell type can be identified by filling the cell with biocytin carried in the

recording pipette followed by post-hoc staining. To understand the synaptic mechanisms that govern translaminar cortical synchrony in behaving mice, I made dual whole-cell recordings in layers 2/3 and 5.

1.7 Aims

In my PhD project, I examined excitatory pyramidal neurons involved in sensory processing in layers 2/3 and 5 in awake, head-fixed mice. I developed a paw tethered system to permit online measurements of paw movement as well as to deliver tactile stimuli to the digits during whole-cell recordings. In this way I

1) Measured basic cellular intrinsic properties of L2/3 and L5 excitatory neurons

2) Correlated sub- and supra-threshold membrane potential activity during different behavioral states

3) Examined sensory processing during different behavioral states

4) Correlated neural responses to digit behaviour.

2. METHODS

All experiments were approved by the Berlin animal ethics committee and carried out in accordance with European animal welfare law.

2.1 Animals and surgery

6-9 week male C57BL6J mice were head implanted with a light-weight metal head holder and anesthetized with isoflurane (1.5-2.0% in O_2), and injected with the analgesic Metamizol (200mg/kg of animal weight). Eyes blink, paw withdrawal and whisker fluctuation were largely absent. The body temperature was maintained at 37 ℃ with a heating blanket and rectal probe. To implant a head support the skin over skull removed and exposed skull area was gently cleaned. The head holder was glued to the skull with superglue (Henkel) and a mini recording chamber (10mm) made with dental cement was centered on the SI forepaw cortex. After implanting head post, animals were returned to their home cage to recover from surgery with 200 mg Metamizol/mL water for drinking.

After 24 hours recovery periods, the animals were progressively habituated to head-restraining. The duration of habituation was increased gradually in daily sessions. The weight of animals was monitored everyday. On the day for experiment, either one or two small craniotomies were made, after surgery, animals were returned to home cage for about 3 hours recovery before electrophysiology experiments.

2.2 Intrinsic imaging and craniotomy window

Intrinsic signal imaging was performed to localize the SI forepaw cortical region for digit 3. The skull was covered by warm Ringer's solution and the superficial blood vessel pattern and location was captured under 530nm green light with a monochrome CCD camera (QImaging, QIcam Fast 1394) mounted on a stereo microscope, then switch to 630nm red light to imaging the intrinsic signals. Brief tactile stimulations were delivered repeatedly by piezo (10Hz for 8s, 30s per sweep)onto forepaw Digit 3 to evoked an intrinsic signal. The intrinsic signal for Digit 3 in forepaw SI was then matched with the blood vessel patterns captured under green light to guide the craniotomy.

On the day of experiment, animals were anesthetized with isoflurane (1.5-2% in O_2). Two small neighboring craniotomies (~0.5mm^2) were made for dual whole-cell recordings, one was right over the signal region for SI forepaw D3, and the other one was lateral. For single recordings, only one craniotomy was made right over intrinsic signal.

2.3 Electrophysiology

The membrane potential of cortical neuron was recorded in whole-cell current clamp mode. Patch pipettes were made from 2-mm borosilicate glass pipettes (Hilgenberg) with a resistance of 5-7 MΩ, and filled with intracellular solution containing (in mM): 135 potassium gluconate, 4 KCl, 10 HEPES, 10 phosphocreatine, 4 MgATP, 0.3 Na_3GTP (adjusted to pH 7.3 with KOH), and 2mg/ml biocytin. The Ringer's solution used to cover the skull and craniotomy containing(in mM): 135 NaCl, 5 KCl, 5 HEPES, 1.8 $CaCl_2$, 1 $MgCl_2$. Whole-

cell current-clamp recordings were acquired by an Axon Multiclamp 700B amplifier (Molecular Devices). The membrane potential recordings were low pass filtered at 10 kHz and digitized at 20 kHz via an ITC-18(HEKA) analog to digital interface board connected to a PC under the control of script running by IGOR Pro (Wavemetrics).

Whole cell recordings were obtained in blind mode (Margrie et al., 2002). Pipettes were slowly advanced into cortex through one craniotomy (single recording) or two close craniotomies (dual whole-cell recordings) with a positive pressure (100-300 mbar) while a 10mV square wave was applied to measure the resistance of pipette tip, once the resistance was dramatically increased, the positive pressure was lowered then removed to obtain gigaseal with help of gentle suck, once gigaseal was formed then a second gentle suck was applied to rupture the membrane patch and establish whole-cell recording mode.

2.4 Forepaw digit tracking and stimulation

The right forepaw was tethered to recording platform with insulating paper band. Digits overhung the platform edge. A force-feedback mechanical stimulator with a sensor arm (Aurora Scientific, Dual-Mode Lever Arm systems 300-C) was positioned underneath the Digit 3 (occasionally tip of Digit 2 might touch the edge of sensor). The arm sensor was kept in constant contacting with the digit on the glabrous skin of paw throughout experiment to track the movement of digit on-line and deliver single brief tactile stimuli (2ms). The tactile stimuli were delivered in a pseudo-randomized pattern,

with time interval between stimuli being 2-4 s, and strength was 10 mN. The digit movements and sensory stimuli were recorded and delivered alongside electrophysiology recordings via the ITC-18 A/D board under command of IGOR Pro. Digit movements were spontaneously generated, but could also be triggered by sound and tactile stimuli.

2.5 Cooling system (Thermal touch)

Cooling stimuli were performed with a 3×3 mm Peltier element stimulator (Yale Medical School). A 3 s cooling stimulus (0.5-s onset ramp, 2-s hold, 0.5-s offset ramp) was delivered to the Digits 2–4 on the glabrous skin of forepaw. The amplitude for cooling stimuli was 10℃, the temperature drop from 32 to 22 ℃.

2.6 Histology

After each experiment, mice was anesthetized by intraperitoneal injection of 2.5 g / body weight urethane, then transcardially perfused with phosphate-buffered saline (PBS) then with 4% paraformadehyde (PFA). The brain was removed and kept in 4% PFA overnight after perfusion, then store in PBS for slicing and staining. Brain was sliced in coronal into 100μm thickness using Leica VT1000 S vibrating microtome. Next, slices were transferred to cytochrome oxidase staining and subsequently biocytin staining which was processed by ABC kit (Vectastain). Stained slices were mounted in Moviol and stored at 4°C in fridge. Stained cells were photographed and reconstructed using NeuroLucida software (MicroBrightField).

2.7 Data analysis

Data were analyzed using custom made scripts in IGOR Pro and Matlab.

All data with mean value are shown in mean ± SEM.

After hyperpolarization (AHP)

The AHP was calculated as the difference between the baseline of mean V_m at 150-50ms before current injection and the most negative mean V_m peak (±0.5 ms) in 100 ms post-injection.

Input resistance

Negative current pulses (100 ms, 100pA) were injected at the beginning of whole-cell recording to measure the input resistance. The change of V_m due to access resistance during input resistance measurements was corrected from V_m off-line (Crochet & Petersen, 2006). Since the charging time course of access resistance was about 2 ms, an exponential curve was fitted from 2.5 ms after current injection to 60 ms to avoid access charging, then the V_m difference from start point of current injection to the bottom part (e.g. 60 ms) along the fitting wave was taken as the V_m difference caused by input resistance.

Spike triggered averaging

Action potentials (APs) were sorted from quiet and moving periods then aligned to their peak V_m value time point. AP threshold was measured as peak of the triple differentiated AP. The pre-spike depolarization leading to an AP was measured as the liner fit in V_m trajectory in 22–2 ms before AP peak.

Selection of behaviour states

Movement and quietness periods were selected based on the digit tracking traces ($digit_{beh}$). To measure digit movement we firstly applied a sliding 50 ms window average on digit tracking trace (smooth trace) and then calculated its first derivative. Movement onsets and offsets were detected by thresholding the rectified first derivative of the smoothed digit tracking trace. A low threshold (0.5–2 SD of the rectified first derivative of the digit tracking trace) was applied to reliably detect even small/brief movements. In some cases this low threshold resulted in the detection of multiple movement onsets/ offsets during long digit movements. To extract only one movement onset and offset in these cases, all onsets/offsets that were less than 500 ms apart were discarded. Quietness periods were excluded when a moving state is neighbored within 1 s.

Resting/moving

2s epochs of quiet and moving periods were used to characterize the V_m properties (mean, SD, FFT, AP rates, AP threshold, correlation, coherence) shown in Figures 2 and 4. The mean number of epochs/cell was 110.51 ± 10.84 for quiet and 19.45 ± 2.26 for moving. To characterize the frequency spectrum of the V_m, APs were truncated using a median filter then calculated the Fast Fourier Transform (FFT) of the baseline subtracted V_m using the FFT function in Matlab. The power of the FFT at low frequencies was measured as the area under the FFT between 1–5 Hz. Cross correlation analysis between cells by pair recording was made after the V_m had been baseline subtracted and normalized by the SD. The coherence between pairs of cells was calculated using:

$$Cxy(f) = \frac{|Sxy(f)|^2}{Sxx(f) * Syy(f)}$$

with Sxx and Syy being the power spectra of the two V_m's and Sxy the crosss-pectrum. The analysis shown in Figure 2H was done for the entire dataset, i.e., the data of quiet and moving periods were pooled together. Here the average V_m of the highly depolarized membrane (Max V_m) was estimated by averaging the 10% of most depolarized V_m values.

Slow frequencies events

To characterize the slow frequencies events (SFEs) during quietness we sorted quite epochs in 4 s. To detect the onsets and offsets of the SFEs (Figure 5, 7) the V_m were smoothed (averaging bin: 25 ms), we next thresholded the smoothed V_m at 25% – 30% of the distance (V_m range) between the Min V_m and the Max V_m. Min and Max V_m were calculated from the 5% most hyperpolarized or depolarized V_m values respectively. We analyzed SFEs with a duration longer than 100 ms and an average V_m between onset and offset larger than 60% of the V_m distance. Moreover, we excluded events that were preceded by another depolarizing event in less than 100 ms. To measure the grand average of the onsets and offsets of the SFEs we aligned all events to threshold crossing. To measure the latency between the L2/3 and L5 cell pair at the onset and offset of depolarizing events we fitted each pair trials around the onset or offset (± 100 ms) with a sigmoidal function. The latency was then estimated from the differences between time points at the 5% level of the fits. We included only onsets and offsets in which the fits of

both L2/3 and L5 had a goodness-of-fit > 0.6. To calculate the average frequency and duration of SFEs (Figure 6), threshold crossings that were less than 50 ms apart were excluded to avoid that large but transient fluctuations during SFEs were counted as separate events, then frequency of the SFEs was given as the number of threshold crossings per second.

Movement onset

To analyze the membrane potential dynamics around the onset of a digit movement movement onsets were sorted using the method described above. In this analysis we included all movements, irrespective of their amplitudes and durations. The latency between the $digit_{beh}$ and V_m was then estimated by the lag of the peak in the cross correlogram between the $digit_{beh}$ and V_m around the movement onset (–200 ms to 100 ms). V_m variance after movement onset was estimated by calculating the variance of the V_m in a 200 ms window across trials before (–600 to –400 ms) and around the peak after movement onset (~50 to 250 ms, gray shaded areas in Figure 11E), The bin for APs PSTH is 40 ms.

Tactile response

To classify the behavioral state during tactile stimulation we calculated the movement of the $digit_{beh}$ from the rectified movement traces in 300 ms window pre/post tactile stimulation. Using these two measurements we then classified each trial into three categories: Quiet-Quiet(QQ) = no movements before and after tactile stimulation, Quiet-Move(QM) = no movements before but movements after tactile stimulation, Move-Move(MM) = movements before and after stimulation. Trials with movements before but not after sensory

stimulation were excluded from the analysis. No movement was defined as amplitudes < 1.5*median of all amplitudes and movements were defined as amplitudes > 2.5*median of all amplitudes.

The amplitude of tactile responses (Figures 12E and 15D) was measured as the difference between the V_m at stimulus onset and the V_m at the peak of the synaptic response. The latency (Figure 12I) was estimated by fitting a sigmoidal function to the average evoked response between stimulus onset and the peak of the response. The time at 3% of the amplitude was set as onset latency of response. To measure the trial-by-trial correlation between the tactile-evoked responses of simultaneously recorded cell pairs (Figures 12J and 12K) the Pearson correlation coefficient was measured between the amplitudes of paired cells.

The reversal potential (V_{rev}) of tactile-evoked response was calculated by two complementary methods. First, the responses amplitude versus the pre-stimulus V_m was plotted with a linear regression. For this we fitted a line into the plot of amplitude versus pre-stimulus V_m. As the V_m at which the response amplitude was 0 mV was taken as the reversal potential. In addition, we measured V_{rev} by the peak of the averaged tactile-evoked response. This method resulted in almost exactly the same estimates of V_{rev}, as compared to the line-fitting method (correlation = 0.97, p = 0, mean difference between fit and peak = 1.00 ± 0.15 mV).

The tactile-evoked suprathreshold response was measured as the firing rates in 100 ms window after stimulus onset (0–100 ms) with the baseline APs rate subtracted (baseline firing rate was measured in a 100 ms window before

stimulus onset). The APs rate in a window from 300 to 400 ms after stimulus onset was measured as the evoked suprathreshold response in the late phase of the tactile response, the baseline APs rate was subtracted as well. To show the relationship between the evoked firing rates and the ΔV_m between AP threshold and V_{rev}, we measured the APs rate in the 100 ms after the tactile stimuli.

The average V_m during the pre-stimulus phase was calculated in a 100 ms window before stimulus onset (from –100 ms to 0 ms), and the average V_m of the late phase was calculated from 300 to 400 ms after stimulus onset.

3 RESULTS

3.1 Layer-specific neural circuit dynamics in SI of awake mice

3.1.1 Cellular properties for L2/3 and L5 neurons in awake mice

Blind *in vivo* whole-cell current-clamp recordings were targeted to cells in the L2/3 and L5 in the digit 3 representation of primary somatosensory cortex (SI), permitting measurements of intrinsic membrane properties and membrane potential dynamics. Recordings were obtained using the experimental setup shown in Figure 1A. The mouse was positioned on a platform with the head restrained and the right forepaw gently tethered onto the platform. Digits of right forepaw hung over the edge of platform and were able to move relatively freely. The cells that were recorded were located between 121.65 and 384.42 μm for L2/3 (mean depth 245.30±17.91 μm), and between 538 and 823.8 μm for L5 (mean depth 649.43±14.28 μm) under the pia (Figure 1B). The measurements of cell depth and cell type were read from the scale on the micro-manipulator and in a subset of recordings confirmed by post-hoc biocytin staining (L2/3 = 4/17 and L5 = 15/28 neurons).

The intrinsic membrane potential properties were measured immediately after break-in during quiet wakefulness. Neurons in L5 were more excitable than L2/3, as shown by the generation of more action potentials (APs) with equivalent currents injections, and APs could be evoked at lower currents in L5 compared to L2/3 neurons (Figure 1C, D). The higher levels of excitation

in L5 might be due to their higher input resistance (Figure 1E, mean: $L5_{IR}$=51.65±3.35 MΩ, $L2/3_{IR}$=33.46±2.80 MΩ, P<0.001). Furthermore, another distinct characteristic appears in L5 neurons after the injection of a current. Following each step of positive current, L5 neurons showed an after-

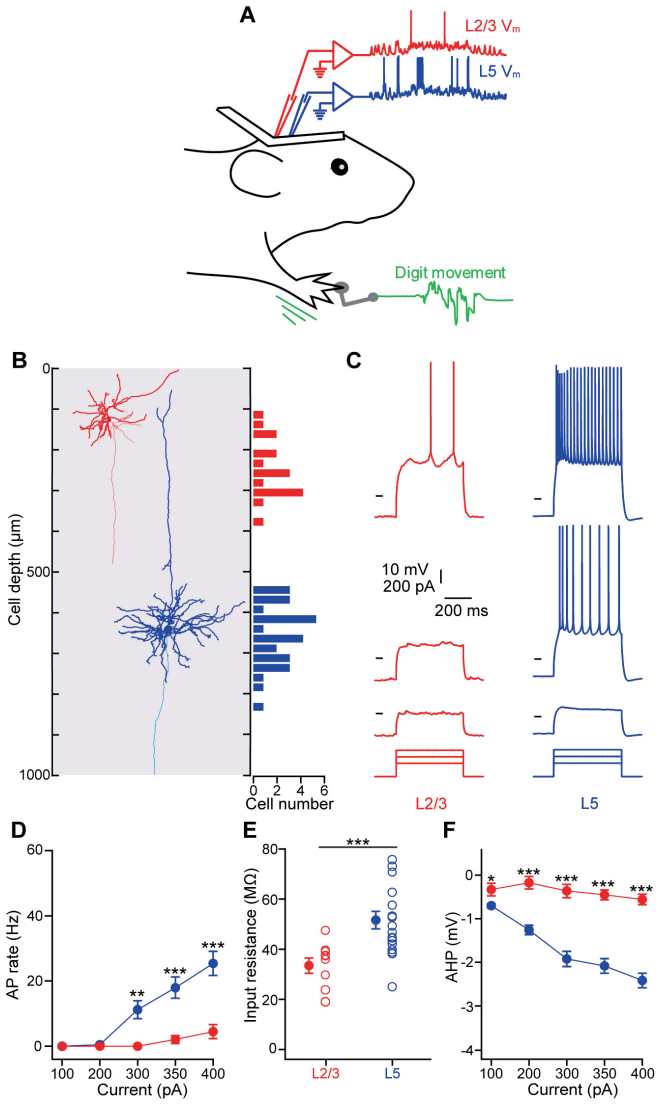

Figure 1. Intrinsic electrophysiology properties of pyramid neurons in L2/3 and L5
(A) Schematic experimental setup showing head-restrained awake mouse with recording electrodes and digit tracking/stimulation sensor (grey). An example tracking trial shows in green.
(B) Examples of reconstruction of post-hoc biocytin-stained L2/3(red) and L5(blue) neurons, with distribution histogram of recorded cell depth(L2/3 n=17, L5 n=28).
(C) Currents injection evoked excitation during *in vivo* whole-cell recording from a L2/3 (red) and L5 neuron (blue).
(D) The currents injection and corresponding number of evoked action potential for L2/3(n=12) and L5 (n=21).
(E) Input resistance for neurons in L2/3 were smaller than L5.L2/3(n=11), L5(n=18)
(F) The amplitude of after hyperpolarization potentials (AHP) for L5 neurons enhanced with larger currents injection, comparing to those of L2/3. (L2/3, n=10; L5, n=22)

hyperpolarization (AHP) in the V_m. While the amplitude of AHP increased with injection, AHP was nearly absent in L2/3 neurons after the termination of each injection step (Figure 1F, at 400pA, $L5_{AHP}$ vs $L2/3_{AHP}$, $P<0.001$).

Overall, in awake animals, SI L5 neurons exhibit stronger excitation, a larger input resistance and AHP than L2/3 neurons, which suggest intrinsic membrane properties distinct from those of L2/3 neurons.

3.1.2 Membrane potential dynamics of L2/3 and L5

Membrane potential (V_m) dynamics in awake animals are more complex than in anesthetized animals. To study how cortical activities interacts with behaviour, while recording cellular V_m, a force-feedback sensor was positioned underneath forepaw digit 3, maintaining continuous contact to track its movement. Digit movement measured by the sensor provided a definition of quiet wakefulness (Q) and movement (M) states. This allowed us to correlate digit movement with membrane potential activities in the SI of forepaw.

During quiet wakefulness, the cerebral cortex in mice is characterized as having large amplitude, slow frequency oscillations as shown by the local field potential (Crochet & Petersen, 2006; Poulet & Petersen, 2008). Single and dual whole-cell current-clamp recordings from cells in L2/3 and L5 showed similar features (Figure 2A), but neurons in L5 presented higher firing rates than those of L2/3 (Figure 2E, $L2/3_{FR}$, Q = 0.32 ± 0.10 Hz, n = 12 cells vs. $L5_{FR}$, Q = 2.86 ±0.60 Hz, n = 19 cells; $P<0.001$), which might partially be due to its more depolarized membrane potential (Figure 2G,

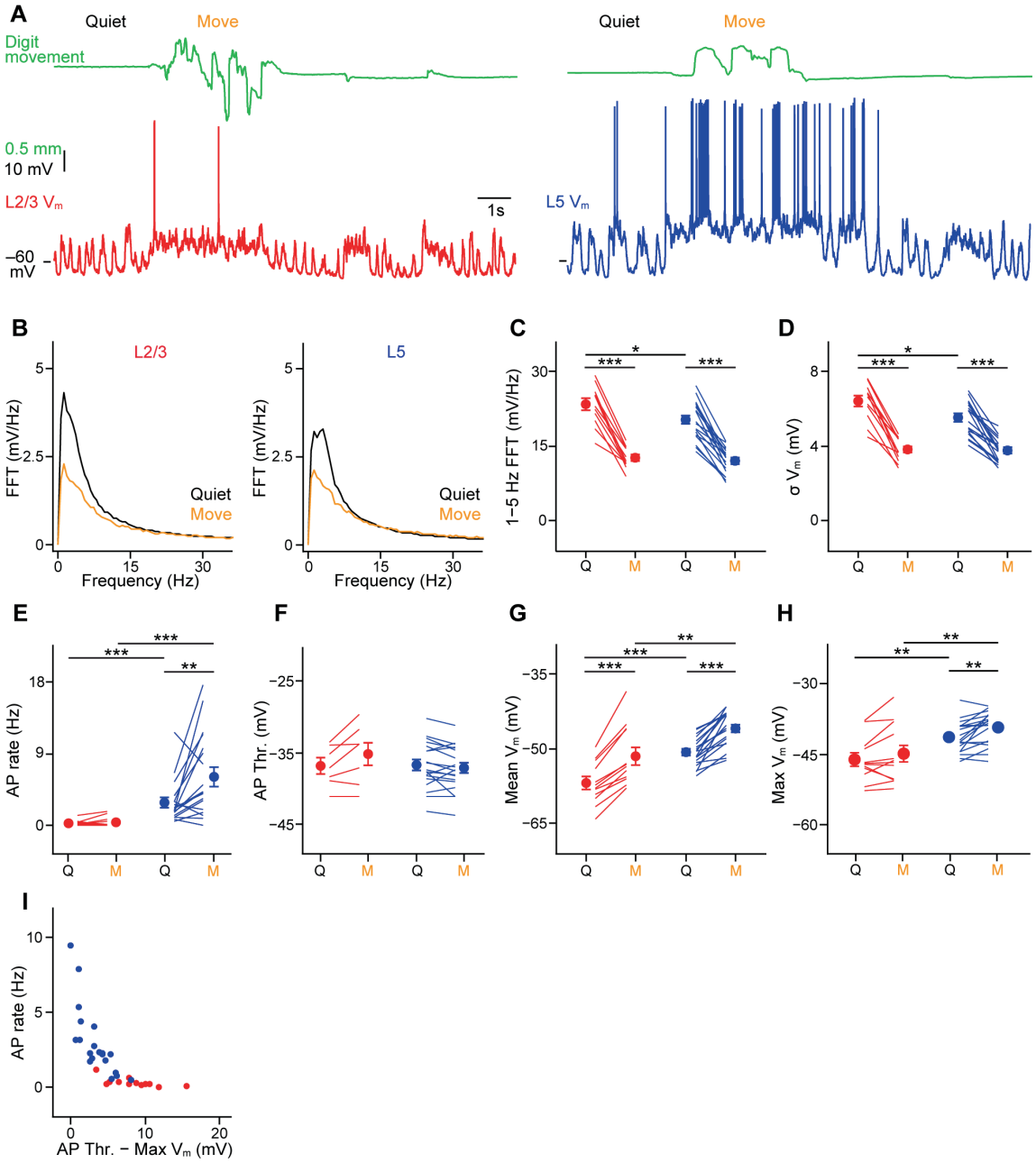

Figure 2. Membrane potential (V_m) dynamics in layer 2/3(L2/3) and layer5(L5) during Quietness(Q) and Movement(M)

(A) Whole-cell recordings on a L2/3(red) and a L5(blue) pyramidal neurons during quietness and movement. Top lime trace: tracking digit behaviour.

(B) Averaged FFT from L2/3 and L5 membrane potential, Low frequency FFT for both of L2/3 and L5 are depressed during “Move”period.

(C) The amplitude of 1-5 Hz frequency power of FFT for L2/3 and L5 during “Quiet” and “Move”. 1-5 Hz frequency FFT of membrane potential in both L2/3 and L5 show higher power during “Quiet” period.

(D) Vm standard deviation is decreased in both L2/3 and L5.

(E) Firing rates changes in L2/3 and L5 during Quiet and Move periods.

(F) AP threshold between L2/3 and L5 kept similar during Quiet and Move periods.

(G) V_m became strongly depolarized during “Move” for both layers. L5 is more depolarized than L2/3 during both Quiet and Move periods.

(H) L5 neuron showed most depolarized V_m in both behaviour states.

(I) Mean firing rates plotted with the distance between spike threshold and most depolarized V_m.

L2/3 n=12, L5 n=19. Data in C–H are means± SEM(* P<0.05;** P<0.01;*** P<0.001)

mean: L2/3 V_m =–56.9 mV, L5 V_m =–50.70 mV, P<0.001).

With the start of a continuous movement of the forepaw, there were accompanying changes in the brain state in both layers. The sub-threshold V_m displayed a depolarized membrane potential during movement (Figure 2G; L2/3 V_m Q = –56.92 ± 1.21 mV vs. M = –51.45 ± 1.73 mV, n = 12 cells, P < 0.001; L5 V_m Q =–50.70 ± 0.65 mV vs. M =–45.89 ± 0.80 mV; n = 19 cells, P <0.001). Membrane potential fluctuations in both layers showed a reduction of power in the low frequency band, a significant drop highlighted by Fast Fourier Transform analysis (FFT) for V_m (1–5Hz) (Figure 2B and 2C). Meanwhile, the standard deviation of the sub-threshold V_m decreased as well (Figure.2D, mean: $QL5_{SD}$=5.50 mV, $ML5_{SD}$=3.77 mV, Q vs. M, P<0.001; $QL2/3_{SD}$=6.395 mV, $ML2/3_{SD}$=3.80 mV, Q vs. M, P<0.001). This suggests that variations of sub-threshold V_m in both layers (or SI forepaw) are governed by the same rule.

An examination of supra-threshold activity showed that AP rates increased in L5 neurons but not significantly for those of L2/3 (Figure 2E, $L5_{AP}$ M=6.14 ± 1.16 Hz, $L2/3_{AP}$ M=0.45 ± 0.18 Hz, $Q_{L2/3}$ vs. $M_{L2/3}$, P=0.851; Q_{L5} vs. M_{L5}, P=0.005). In addition, the temporal dynamics of APs showed a skewed distribution of inter-spike intervals in both L2/3 and L5. 22% of L2/3 APs and 30% of L5 APs exhibited temporal intervals below 25 ms which we termed a burst (Figure 3). Meanwhile, the proportion of bursts in APs was, overall, higher in L5, but no significant differences between periods of quiet and movement were detected (Figure 3, Burst frequency $L2/3_{BF}$, Q = 0.02 ± 0.004 Hz, M = 0.03 ± 0.01 Hz, n = 13 cells vs. $L5_{BF}$, Q = 0.14 ± 0.05 Hz, M = 0.25 ±

0.12 Hz, n = 23 cells. L2/3 vs. L5 Q, P = 0.019). Thus supra-threshold activity does not seem to follow the pattern governing sub-threshold behavior.

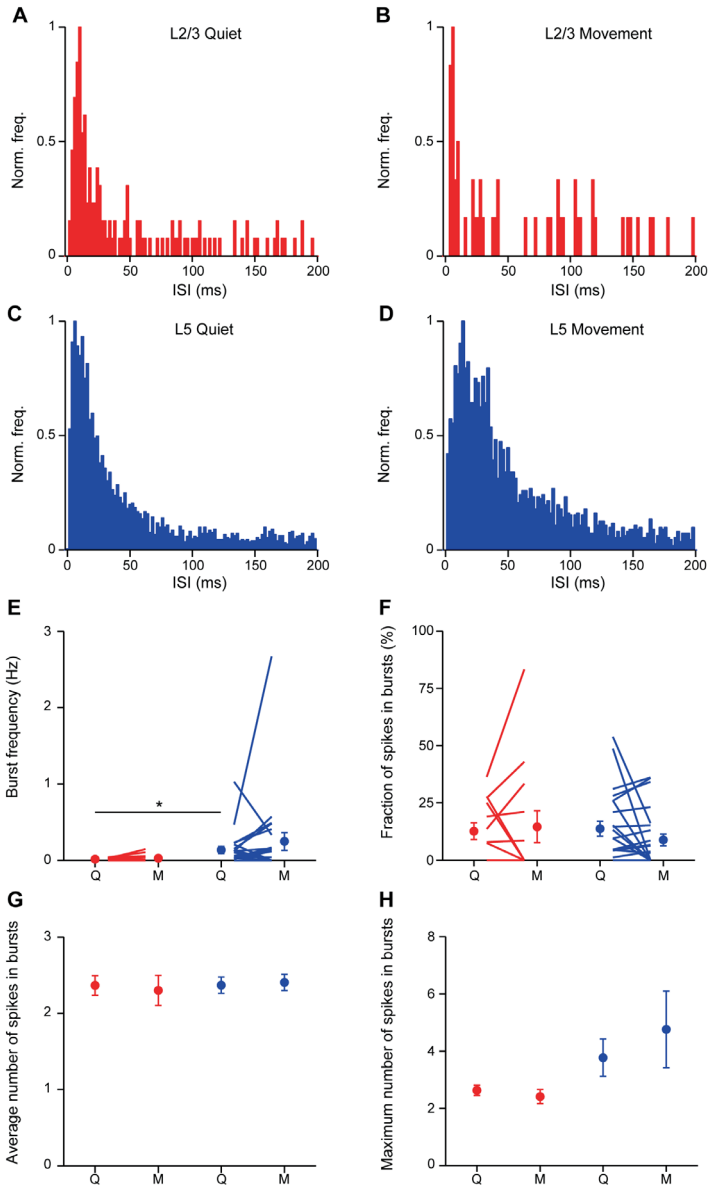

Figure 3. Inter-spike-intervals of spontaneous action potential in bursting.
(A) Distribution of inter-spike interval (ISI) of APs in L2/3 neurons during quietness periods.
(B) Distribution of inter-spike interval (ISI) of APs in L2/3 neurons during movement periods.
(C) Same as (A) but for L5 neurons.
(D) Same as (B) but for L5 neurons.
(E) APs burst frequencies in L2/3 and L5 neurons during quietness and movement periods. Lines show individual cells. See methods for burst classification.
(F) Fraction of bursting APs in all APs in L2/3 and L5 neurons during quietness and movement periods.
(G) Mean number of APs in a burst is similar in L2/3 and L5 neurons.
(H) Maximum number of APs in a burst in L2/3 and L5 neurons.
Filled circles with error bars show mean ± SEM.

This seemed like an exception to the normal behavior of APs and merited a deeper examination. First we compared AP thresholds in states of quiet and movement. AP thresholds did not exhibit significant differences between states or across layers (Figure 2F, $QL5_{thr.}$=–36.75 mV, $ML5_{thr.}$=–37.16 mV, P=0.17; $QL2/3_{thr.}$=–36.89 mV, $ML2/3_{thr.}$=–35.25 mV, P=0.10; QL5 v.s QL2/3, P=0.86; $ML5_{thr.}$ v.s $ML2/3_{thr,}$ P=0.24). This implied that the threshold is a basic, relatively stable property of neurons in both L2/3 and L5. Next we measured the pre-threshold membrane potential, the max 10% of V_m (sub-threshold) distribution sorted out a slight but significant increase in L5 neurons during movement (Figure 2H, M_L5V_mMax=–39.41mV, Q_L5V_mMax=–41.33 mV, P=0.003; M_L2/3V_mMax=–44.97 mV, Q_L2/3V_mMax=–46.14 mV, P=0.07). This indicated that the depolarization in L5 V_m is much closer to the threshold than that of L2/3 during movement, which would help to raise the probability of spiking in L5 neurons. Furthermore, plotting differences between the threshold and the max 10% V_m with AP rates indicated a conspicuous exponential relationship (Figure 2I). The rising slope consisted entirely of L5 neurons, whereas L2/3 neurons were almost absent; most of them contributed to the basal phase, along with a small proportion of L5 neurons. The larger input resistance and higher levels of depolarized V_m create a situation in which excitatory synaptic inputs would be more likely to trigger APs in L5 than in L2/3 in awake behaving mice. I believe that this accounts for its higher rate of L5 neurons.

3.1.3 Behaviour modulate membrane potential synchrony in cortical circuits

Synchrony is a salient feature of cortical activity in both awake and anesthetized animals. It coordinates neural activity across different parts of the brain and helps the neural activity of one brain region become integrated with that of others, which makes our cognition base on a comprehensive information-processing. Synchronous activity has been observed across many brain regions since the development of Electroencephalography (EEG) recordings decades ago. In the SI barrel cortex, the activity of neighboring neurons in L2/3 is highly coordinated during animal quietness (Poulet & Petersen, 2008). It was unknown whether activity across other cortical layers would behave this way. To test whether intracellular membrane potentials exhibit dynamic synchronicity across cortical layers, we performed dual whole-cell recordings within the L2/3 and L5 of the forepaw SI (Figure 4A). When digital activity is quiet, there is a high cross-correlation of V_m between L5 to L2/3 due to highly synchronized, large amplitude slow oscillations that occur across layers (Figure 4B, D, E). In contrast, during digit movement we observed a reduction of V_m synchrony between L2/3 and L5 in all recorded pairs of neurons (Figure 4B, D, E). Thus the neural synchrony exhibited by V_m in L2/3 and L5 neurons in the forepaw SI is dependent on the behavioral state; neural synchrony might be used as a means of defining behaviour states. Interestingly, during quietness, we observed a great lag in peak times across the layers. This suggests that the V_m in L5 leads the phase of slow

frequency fluctuations (Figure 4E), while during movement, peak time lag was diminished (Q, 8.04 ± 1.40 ms; M, 4.35 ± 1.85 ms, P<0.05).

To investigate why there is a drop in correlation during movement, we applied coherence analysis to the same dataset (Figure 4C, G, H). It revealed that coherence dropped dramatically in low frequency band in a way that is consistent with the FFT analysis. This suggests that slow frequency

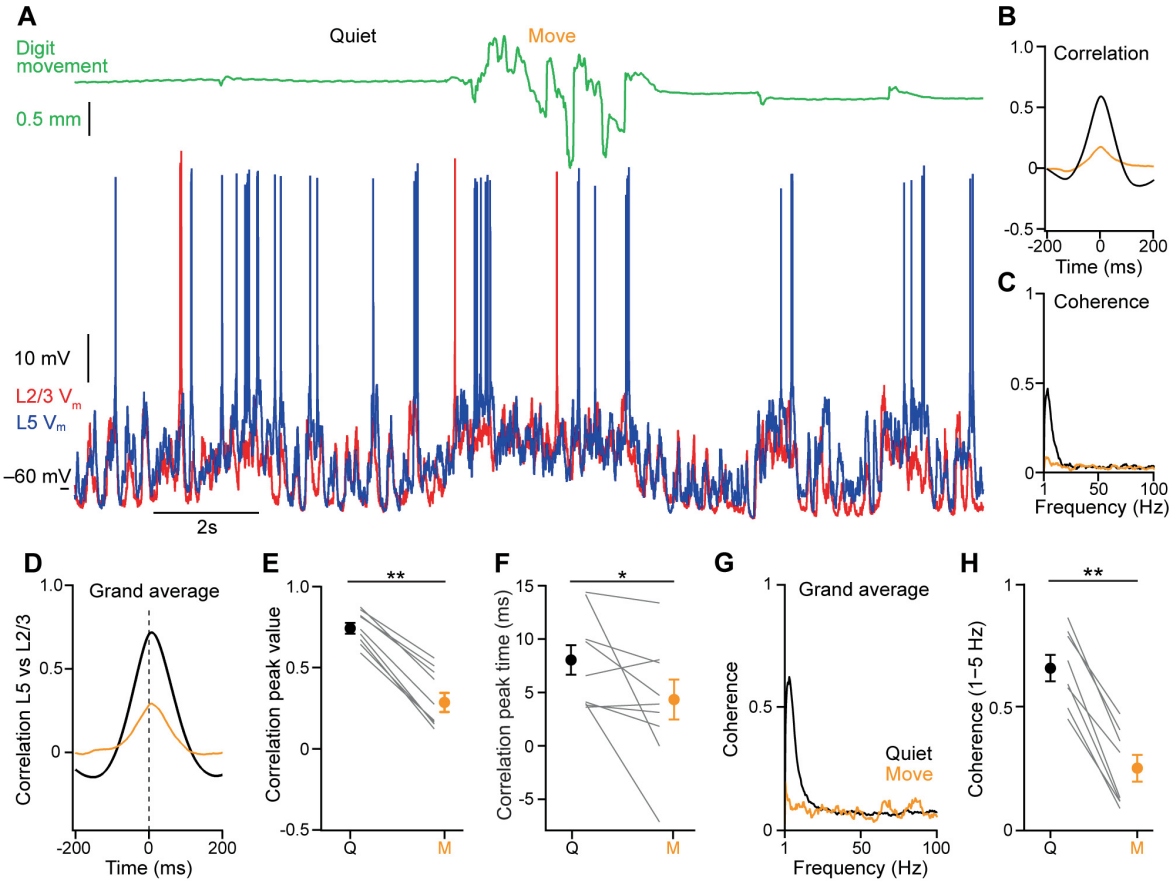

Figure 4. Membrane potential (V_m) synchrony between L2/3 and L5 neurons during Quiteness (Q) and Movement (M)
(A) Simultaneous dual whole-cell recordings on a L2/3(red) and a L5(blue) pyramidal neurons during quietness and movement. Top trace: tracking digit displacement.
(B) Cross correlation for example pair recording in (A).
(C) Coherence spectrum for example pair recording in (A).
(D) Overlaid grand mean cross correlation of V_m from L5 and L2/3 for Q and M period. Correlation decreased during M with respect to Q period.
(E) Peak values of cross-correlation were increased during Q than M P<0.01(P=0.001);
(F) Peak time of cross-correlation exhibit a forward shift during Q suggesting L5 lead the phase of V_m fluctuation. P<0.05(P=0.01)
(G) Overlaid grand mean coherence of V_m in L5 and L2/3 cells for Q and M period.
(H) Coherence of V_m in L5 and L2/3 cells reduced during M in 1–5 Hz frequency band.

fluctuations plays an important role in maintaining the synchronicity of cortical activity. There was also a smaller decrease in the high frequency band. It is very likely that asynchrony during movement is caused by a reduction of coherence in slow oscillations. To quantify differences in timing and other aspects of V_m across layers, we analyzed slow frequency event (SFE) and temporal dynamic relationship between V_m and behavior onset.

3.1.4 Slow oscillations start earlier in L5 than in L2/3

To quantify the time difference between the onset of the SFE in layers 2/3 and 5, we first selected SFEs with clear onset times from our entire collection of dual whole-cell recordings. The SFE was defined as depolarization epochs that surpassed the 60% V_m range between the troughs and peaks of oscillation cycles, with duration of at least 100 ms.

Because the cross-correlation data suggested that SFE onsets occurred earlier in L5 than L2/3, we used L2/3 SFE as a reference to define the relative onset timing for L5 SFE. The examples of onset and offset segments that we selected indicated an earlier onset in L5, while the latency of offset was similar (Figure 5A and 7A). Plotting the V_m of SFE segments with duration in a heat map yielded the distribution of SFE in L2/3 and L5, (Figure 6, mean SFE segments duration L2/3 = 329.06 ± 27.55 ms, n = 13 cells, L5 = 266.94 ± 11.15 ms, n = 23 cells, p = 0.086). This revealed the relationship between the timing and differences in the amplitude of V_m in the L2/3 and L5 neurons (Figure 5B and 7 B). Occasionally, but not often, the V_m in either L2/3 or L5 exhibited an absence of SFE initiation, or an obscure SFE

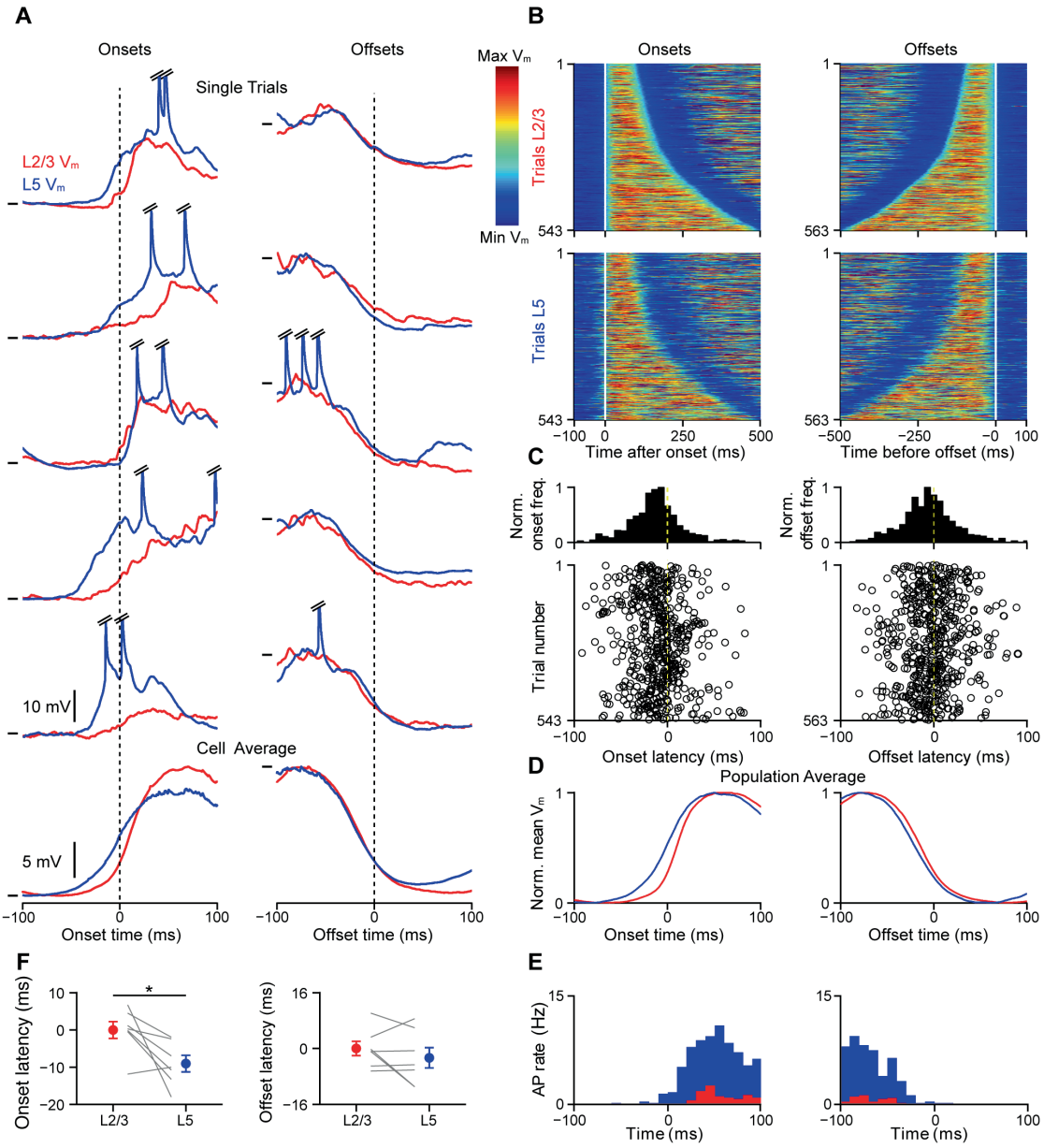

Figure 5. Slow frequency events (SFE) from pair recordings in L2/3 and L5 revealed earlier onset in L5. Analysis triggered on SFE in L2/3.

(A) Examples of SFE segment from a dual whole-cell recordings with mean V_m of all selected segments from example pair(AP truncated). Horizontal marks indicate V_m of L2/3 and L5 (from top) : onset –69.3 / –63.1 mV and offset –47.7 / –44.7 mV; trial 2 onset –59.3 / – 59.1 mV and offset –40.0 / –37.7 mV; trial 3 onset –60.9 / –57.0 mV and offset –31.8 / –31.7 mV; trial 4 onset –59.7 / –56.4 mV and offset –42.0 / –37.7 mV; trial 5 onset –58.3 / –55.7 mV and offset –40.0 / –30.1 mV. Average onset –60.0 / –52.6 mV and offset –41.9 / –37.0 mV.

(B) Threshold-detection based trial-to-trial distribution of V_m SFE in duration.Upper: Onset and offset of aligned Vm SFE in L2/3;Lower: Onset and Offset of V_m SFE in L5 triggered by L2/3.

(C) Up: Normalized timing frequency distribution of Onset and Offset latency. Down: Trial to trial relative latency distribution in L5 regarding to L2/3 exhibit a right skew in Onset but symmetric distribution in Offset.

(D) Normalized grand averaged Vm SFE revealed an earlier relative Onset latency in L5, whereas Offset latency is similar.

(E) Population peri- SFE time histogram of APs from corresponding distribution in(D).

(F) Summary of mean Onset and Offset latency analysis, the mean L2/3 onset/offset time was subtracted the from all values. (onset: mean= –9.334 ms, P=0.03125; offset, mean= –1.1003 ms, P= 0.6875) *P < 0.05, **P < 0.01, ***P < 0.001.

initiation with a shorter duration and smaller amplitude (Figure 8). A trial-to-trial distribution of the differences in onset and offset latency indicated that L5 V_m lead the onsets with a high frequency, whereas the offset latency was quite similar to that of L2/3 (Figure 5C and 7 C). The earlier onset of L5 was clear-cut in a grand normalized average of SFE, while there was no visible difference in offset latency (Figure 5 D and F. Mean onset latency difference 9.07 ± 2.19 ms, P=0.031; offset latency difference was 2.69 ± 2.9 ms, P=0.68). Our analysis showed that this leading pattern described not only exhibiting at the phase of input, the sub-threshold level, but also at the super-threshold V_m of the AP, which was also attained earlier in L5 than in L2/3, as shown in the PSTH graph. But the offset of the two layers phased out at similar time (Figure 5E). However, there is a crucial difference when our analysis set L5 as the reference, SFEs in L5 neurons offset earlier than those in L2/3 as well (Figure 7F). These data reveal that L5 is the leading player in both sub- and supra-threshold activities in the initiation of slow frequency fluctuations.

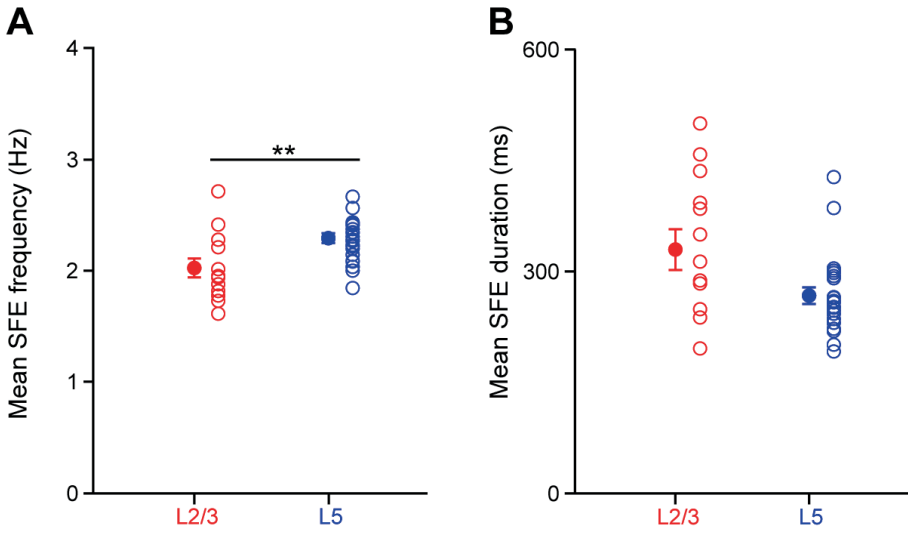

Figure 6. Basic properties of slow oscillation during quiet wakefulness.
(A) The mean frequency of slow oscillations during quiet wakefulness.
(B) The mean duration of single segment in slow oscillation.

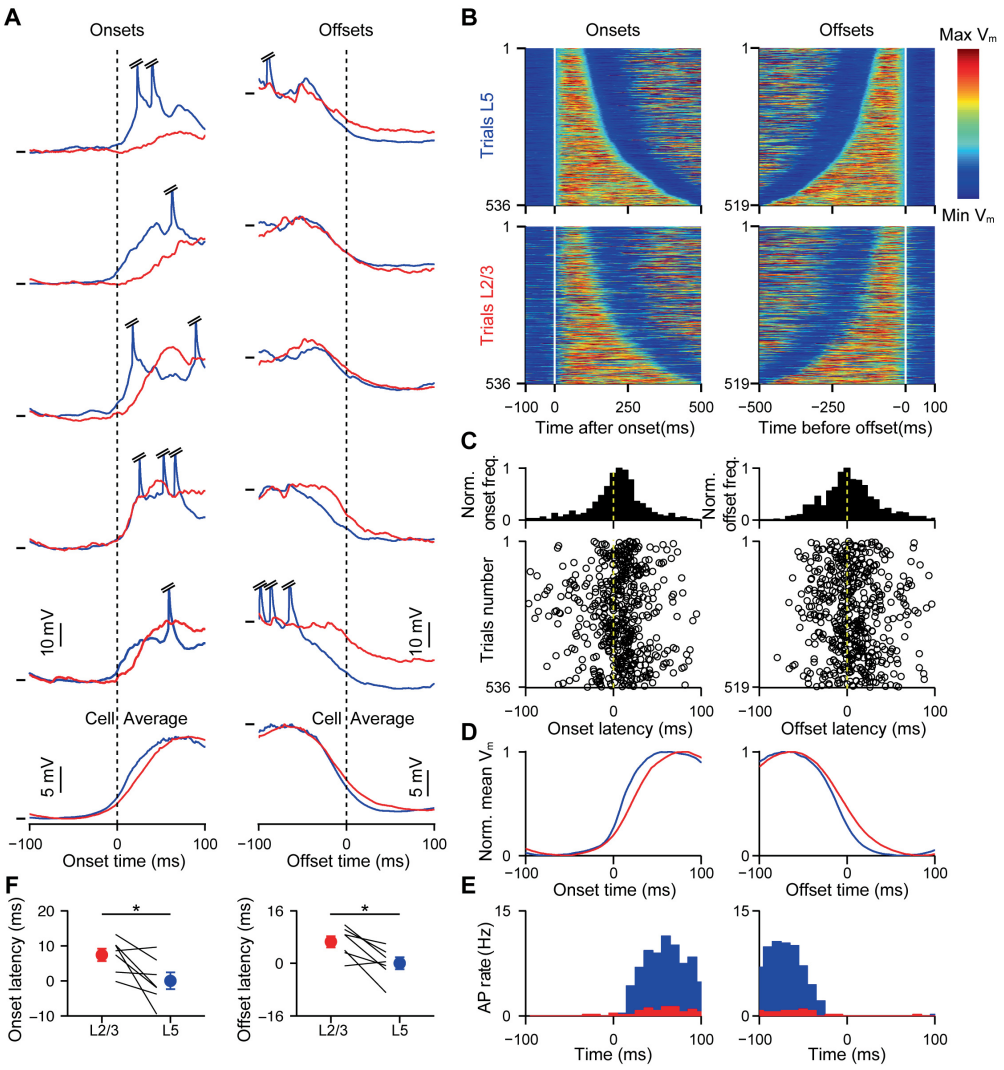

Figure 7. L5 lead slow frequency events (SFE) during quiet wakefulness. Same as Figure 5 but triggered on L5 SFE.

(A) Examples of SFE segment from a dual whole-cell recordings with a mean Vm of all selected segments from respective pairs(spike truncated). Vm traces are aligned to the threshold crossing at onset (left) and offset (right) of the SFE in the L5 neuron, bottom traces show Vm averages. Horizontal marks indicate Vm of L2/3 and L5(from top) : onset –58.9 / – 57.4 mV and offset –44.6 / –39.8 mV; onset –59.7 / –57 mV and offset –44.3 / –38.5 mV; onset –60.5 / –53.0 mV and offset –48.9 / –44.3 mV; onset –58.4 / –47.9 mV and offset –31.2 / –35.2 mV; onset – 56.7 / –48.4 mV and offset –42.5 / –30.9 mV. Average onset –59.7 / 53.1 mV and offset –43.0 / –37.3 mV.

(B) Threshold-detection based trial-to-trial distribution of V_m SFE in duration.Upper: Onset and offset of aligned V_m SFE in L5 ; Lower: Onset and Offset of V_m SFE in L2/3 triggered by L5.

(C) Population distribution (top) and trial-by-trial measurements (open circles, bottom) of the subthreshold onset (left) and offset (right) times in L2/3 neurons relative to the onset and offset times in L5 respectively. Onset and offset times were estimated by the 5% level of a sigmoidal fit to the Vm at onset and offset.

(D) Normalized grand averaged V_m SFE revealed an earlier relative Onset and Offset latency in L5.

(E) Population peri- SFE time histogram of AP times from corresponding data in (D).

(F) Population analysis of onset and offset times triggered on the L5 SFE shows significantly earlier onset and offset times in L5. Data show mean ± SEM. Onset: P= 0.046; Offset: P= 0.031. Note, the mean onset/offset latency of L5 cells was subtracted to highlight the latency difference between L5 and L2/3.

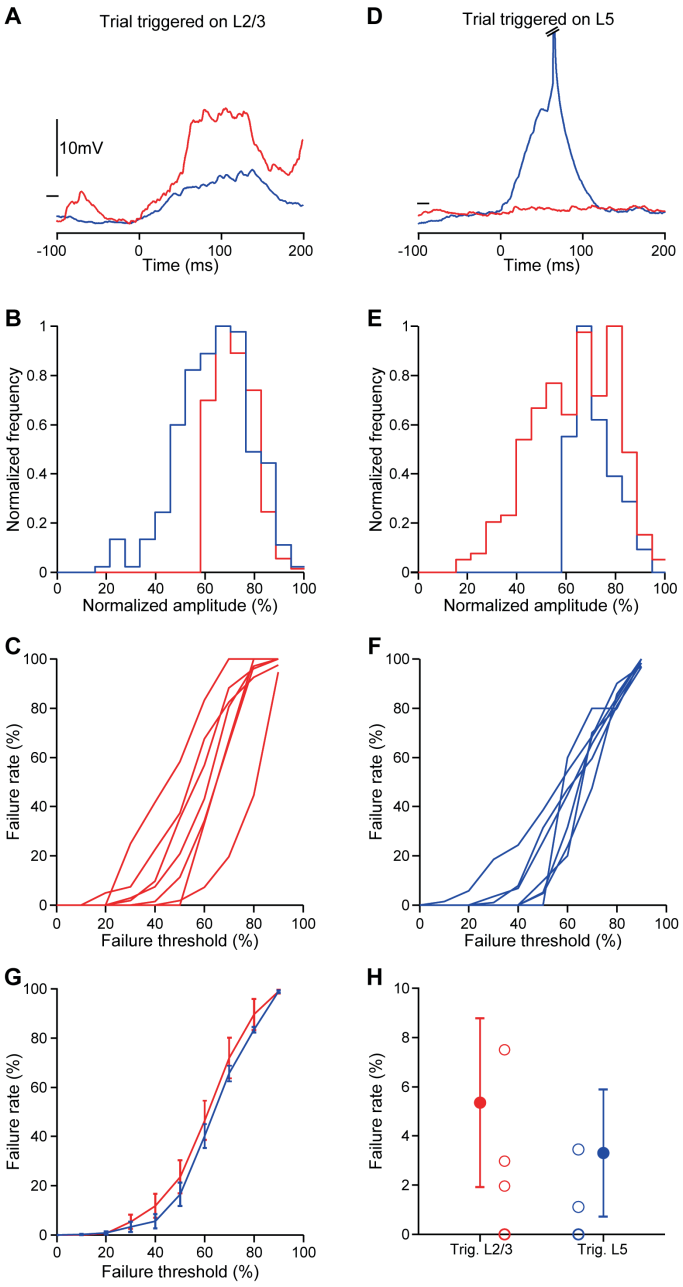

Figure 8. Occasional, small amplitude SFE show failure to initiate in other layer.
(A) Example SFE from a dual recording triggered on the L2/3 activity (red) showing low amplitude event in L5 (blue). Horizontal marks indicate V_m of L2/3 and L5:–60 L5/–65 mV L2/3
(B) Distribution of normalized SFE amplitudes when triggered on L2/3 activity. We analyzed long and large SFE in the triggering cell (normalized amplitude> 60% in L2/3).
(C) Failure rate as a function of failure threshold when triggering on L2/3. Failure threshold was the SFE amplitude in L5 below which a SFE was counted as a failure.
(D) As in (A) but triggered on a L5 SFE. Horizontal marks indicate V_m –60 L5/–68 mV L2/3.
(E) As in (B) but triggered on a L5 SFE. We analyzed long and large SFE in the triggering cell (normalized amplitude > 60%). Note the fraction of low amplitude SFE in L2/3 when triggered on L5.
(F) As in (C) but triggered on a L5 SFE. Failure threshold was the SFE amplitude in L2/3 below which a SFE was counted as a failure.
(G) Population averaged failure rates when triggered on L2/3 (red) and L5 (blue).
(H) Failure rates when triggering on different layers at a failure threshold of 30% amplitude.

3.1.5 Cell-specific action potential firing is built by laminar-specific, synchronized synaptic inputs.

Synchronous AP firing across layers plays a major role in cortical processing. Dual recording data revealed a relationship of "dynamic synchrony" across layers when averaged across 2 seconds segments of SFE. But measurement of fast time scale synchrony of input across layers requires observing the membrane potential dynamics during an AP. Therefore we made spike triggered peri-stimulus time histograms (PSTHs) of spontaneous APs, and analyzed the membrane potential changes during APs in periods of quietness and movement.

When a L2/3 neuron exhibits AP, there is a 6.1% probability that a L5 neuron will fire within a 10 ms window around that event during quietness, which gets to 5.6% during movement. When AP occurs in a L5 neuron, on the other hand, the probability that a L2/3 neuron will fire within this time window is 1.0% during quiet and 0.4% during movement. It is shown that within a fast temporal window, spontaneous APs across layers were evoked asynchronously in a layer-specific way regardless of the behavioral state. This phenomenon had also been shown for neighboring cells within L2/3 (Poulet & Petersen, 2008), where the pattern of inputs was cell-specific.

What is the mechanism of such layer-specific asynchronous AP firing? Then I examined the temporal dynamics of synaptic input driving the AP– the change in V_m just before the onset of the AP. A fast depolarization was

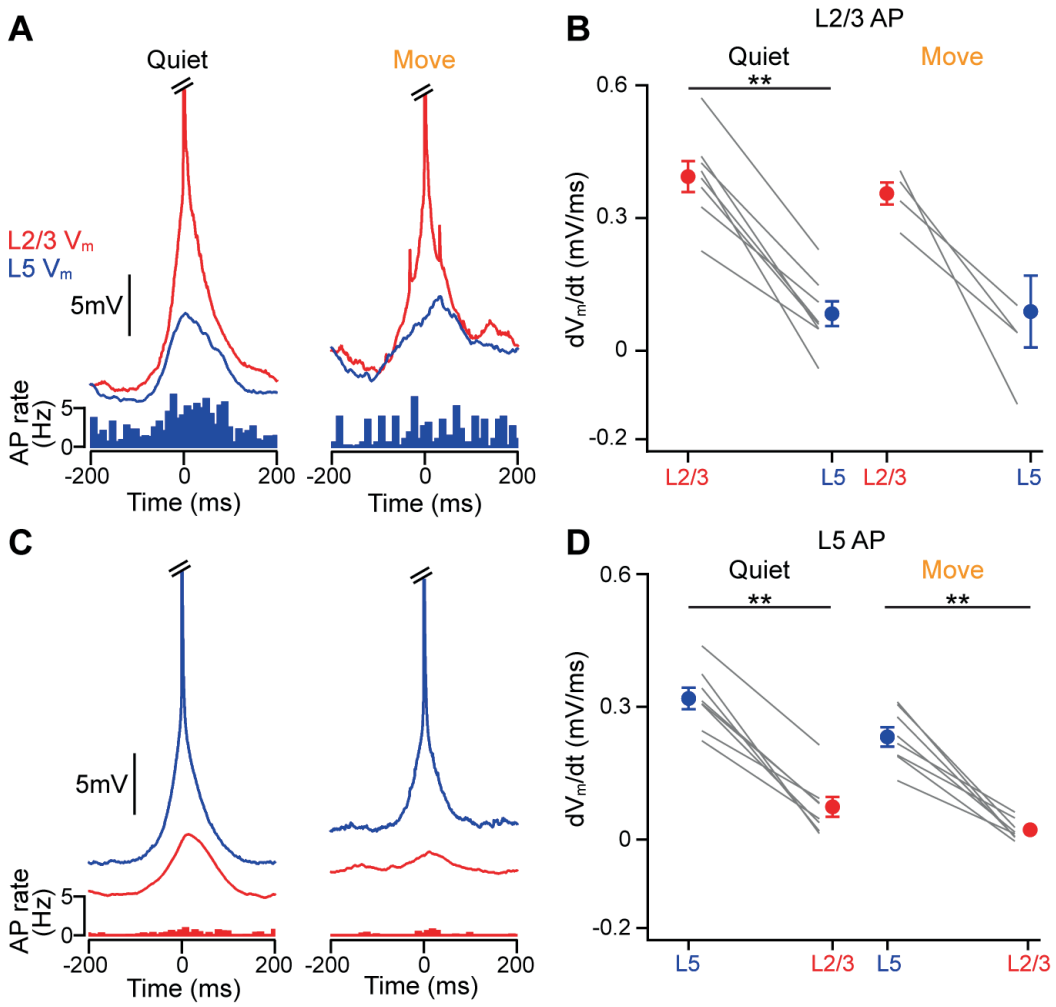

Figure 9. Action potentials are built on layer-specific, large instantaneous excitatory synaptic inputs.
(A) Population average of L2/3 APs (red) and paired L5 neurons V_m (blue) during quiet (left, n = 8 pairs) and moving (right, n = 4 pairs) periods. Bottom histograms show the population AP PSTHs of the corresponding L5 neurons.
(B) Vm trajectory in L2/3 and L5 neurons between –22 ms and –2 ms before a L2/3 AP in quiet and moving periods. Filled circles show population mean with error bars showing mean ± SE.
(C) Same as (A) but for L5 APs average with paired L2/3 V_m and population AP PSTH below (n = 8 pairs).
(D) Same as (B) but with a L5 AP. For all panels *p < 0.05, **p < 0.01, ***p < 0.001.

observed at 22–2 ms prior to the AP peak in the cell that was spiking but not in the simultaneously recorded neuron. It is indicated that spike in each layer drives by an independent input pattern and perhaps source. In the spiking cell both in L2/3 and L5, the speed of the pre-spike depolarization(SP_PreAP) was larger (Figure 9 B and D. Mean SP_PreAP: L2/3, Q=0.39 mV/ms, M=0.35mV/ms; L5, Q=0.31 mV/ms, M= 0.23 mV/ms),

as compared to the non-spiking cell (Mean SP_nonAP: L2/3, Q=0.07mV/ms, M=0.02mV/ms; L5, Q=0.08 mV/ms, M=0.08 mV/ms). Thus our data revealed that within the temporal window of single AP, synaptic input across layers was asynchronous. The cell that fired an AP exhibited a faster ascending rate

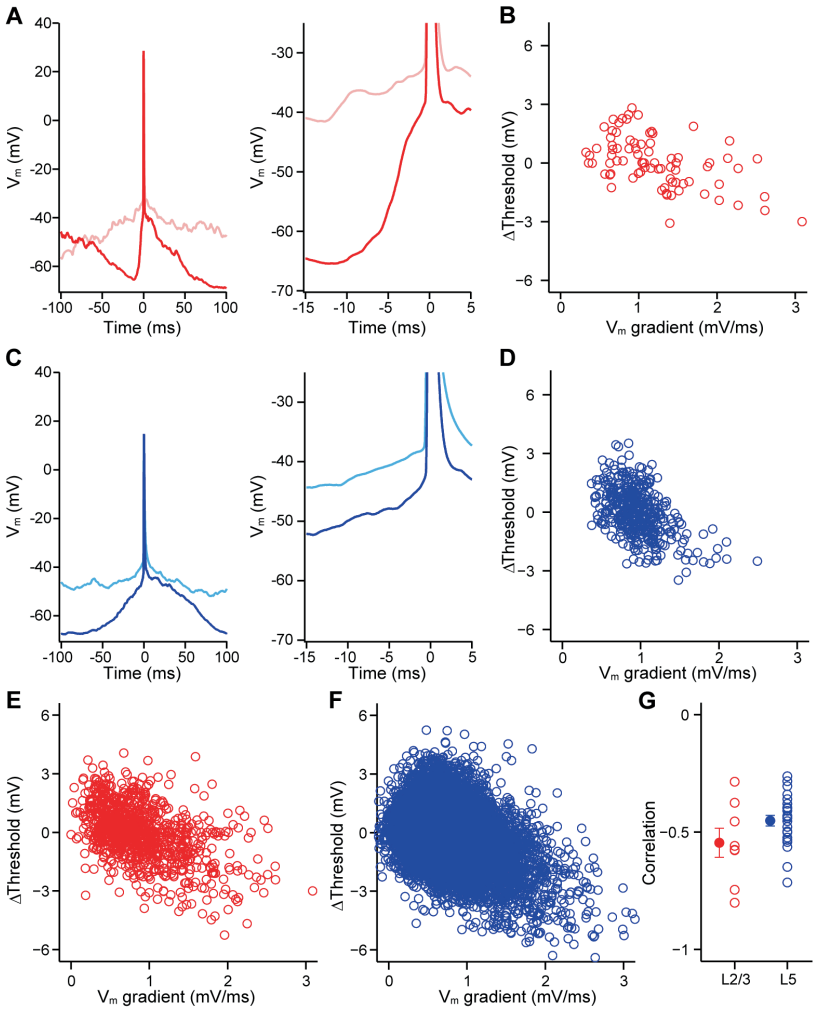

Figure 10. Action potential(AP) threshold is dependent on the ascending rate of pre-AP depolarization in L2/3 and L5.
(A) Left: two overlaid example APs from a L2/3 neuron with different pre-AP Vm trajectory recorded in forepaw SI of an awake mouse. Right: fine temporal resolution of the example APs reveal the relationship between threshold and pre-AP V_m trajectory, with a faster pre-AP depolarization resulting in a lower threshold.
(B) Plot of **Δ**Vm between individual AP threshold and mean threshold, as a function of the gradient of Vm in the 5 ms before AP threshold for cell in example (A).
(C,D) Same as (A,B) but for a L5 neuron.
(E,F) Same as (B,D) but for entire population of L2/3 and L5 APs.
(G) Plot showing the Pearson r correlation coefficient between the change in AP threshold and the pre-spike Vm gradient, open circles represent an individual neurons (L2/3 red, L5 blue).

of pre-spike depolarization than cells that generated normal, non-spiking depolarization.

This also indicated that ascending rates of pre-spike depolarization might be a strong modulator of action potential threshold dynamics (Figure 10) and asynchronous AP firing across layers. These data suggest that within a given brief window of time, synchronous excitatory inputs combine to trigger cell spiking in one layer; if the cell receives fewer inputs, or they arrive in an uncoordinated way, the cell does not spike. In the SI, the patterns that drive action potentials are therefore cell-and layer-specific. This means that within neural circuits, strongly synchronized depolarization network co-exist with other networks that are relatively weakly synchronized, and suggests that 1) networks across layers 2/3 and 5 are sparse connected, 2) network activities are organized in specific and dynamic ways that might be responsible for the fine-tuning of cellular and network processing.

3.1.6 Movement triggered synchronous oscillation onset across layers

In awake animals, synchrony is not only a matter of neural activity inside local circuits; it is also tightly connected to animal behavior. This is reflected in the consistency of behavior in response to neural activation. Our next goal was to measure the synchrony between neural activity at the onset of movement.

To examine V_m activity correlates with the onset of movement, we analyzed the fast dynamics of movement-related synaptic activity at the movement onset. When the forepaw digit of the mouse performed a

spontaneous movement (Figure 11 A), there was a sharp, simultaneous depolarization in both L2/3 and L5 neurons, followed by a rapid reduction in V_m variance 200 ms post onset (Figure 11 E, F). This suggested that excitatory inputs reached both L2/3 and L5 very quickly. Although V_m depolarization was simultaneous in both layers, it did not produce a simultaneous upsurge in firing rates. AP rates in L5 neurons showed a sharp

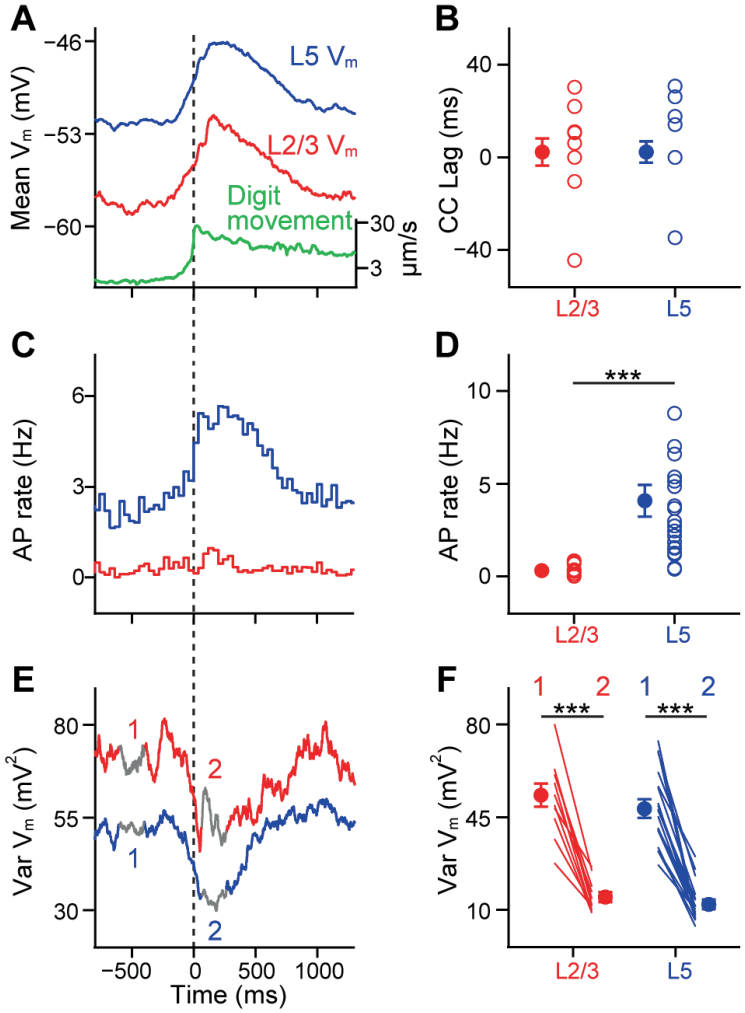

Figure 11. Membrane potential dynamic during spontaneous movement.
(A) Grand average V_m(red and blue) align with rectified first derivative of digit movement onset(green). L2/3 (n=11), L5(n=19).
(B) Cross correlation between V_m and movements to show no timing lag of L2/3 and L5. (P= 0.69747)
(C) Grand AP rates distribution of L2/3(red) and L5(blue) respect to same segments of movement onset.
(D) L5 cells exhibit a much higher AP rates accompanying movement onset (0–1000ms).
(E,F) Averaged V_m variances of movement onset aligned with digit movement.
For all panels *p < 0.05, **p < 0.01, ***p < 0.001.

increment, whereas the AP rates in L2/3 remained similar to those of the pre-movement onset phase (Figure 11 C, D) (L2/3, 0.36 ± 0.08 Hz; L5, 4.25 ± 0.8 Hz, $P<0.001$). Reasons for this difference in AP rates might be the types of local inhibition and excitation-inhibition ratios (E/I) specific to the cortical layers and reflect the fact that L2/3 pyramidal neurons are more hyperpolarized and have lower input resistance.

To illustrate the temporal relationship between digit behavior and V_m, we cross-correlated the V_m from both layers to digit tracking. This displayed the V_m onset latencies that corresponded to digit behavior onset. The peak times of cross correlation for both layers are quite similar (mean: L2/3, 2.25 ms; L5, 2.82 ms) (Figure 11 B). This revealed that subthreshold neural activity is well synchronized with the onset of digit movement across layers.

The observation of simultaneous V_m onset latency in both L2/3 and L5 neurons distinguishes the neural patterns that seen during slow frequency events.

3.1.7 Tactile stimulation triggered correlated sensory responses across cortical layers

A main function of the SI is to process sensory inputs that it receives directly from the thalamus (Meyer et al., 2010a, b). Connectomic studies show that thalamocortical nerves project into the SI in a layer-specific pattern, which strongly indicates that the SI carries out sensory processing in a layer-specific pattern as well. If this is the case, would patterns of layer-specific

processing influence synchrony across different cortical layers and how would behavioral state affect responsiveness?

To address these questions, our next step was to examine the sensory processing properties and synaptic mechanisms in regions of the SI

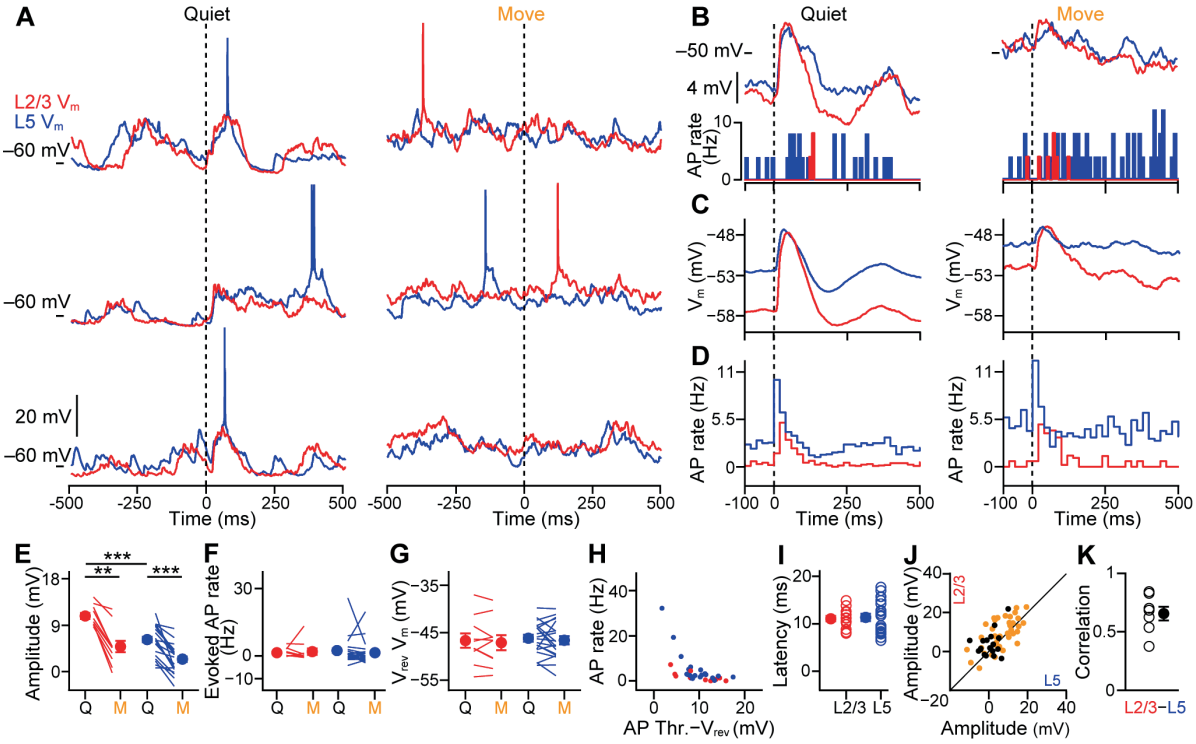

Figure 12. Tactile stimulation to forepaw digit evoke a postsynaptic potential(PSP) in SI L2/3 and L5 neurons during animal quietness and movement.
(A) Example trials of sensory responses from simultaneous dual whole-cell recordings of L2/3 and L5 neurons.
(B) Overlaid mean sensory responses for the pair of neurons in (A). Show tactile stimulated sub-threshold PSP during Quiet(Q) and Move(M) (up), and action potential distribution PSTH within same time window(bottom).
(C) Grand averaged tactile triggered sensory PSP(V_m) in Q and M from all L2/3 and L5 neurons.
(D) Grand averaged peristimulus time histograms(PSTH) of firing rates for Q and M from all L2/3 and L5 neurons.
(E) as indicated in (C), the tactile evoked PSP amplitude decrease in M in both L2/3 and L5 neurons.
(F) Mean firing rates(baseline subtracted) during PSP exhibit no difference between M and Q in both L2/3 and L5 neurons.
(G) Mean PSP reversal potentials are similar for both L2/3 and L5 in Q and M.
(H) Evoked firing rates(100 ms post stimuli onset) plot with the difference between AP threshould and PSP reversal potential. Each filled circle represents a neuron.
(I) Sensory evoked PSP onset latencies indicate no overall difference between L2/3 and L5 neurons.
(J,K) Sensory evoked PSP amplitudes of L2/3 plotted with those of L5 (example pair in A) reveal a highly correlation across two layers(K). Each circle in (K) represent a pair recording.
Filled circles with error bars show mean ± SEM. (* P<0.05; ** P<0.01; *** P<0.001)

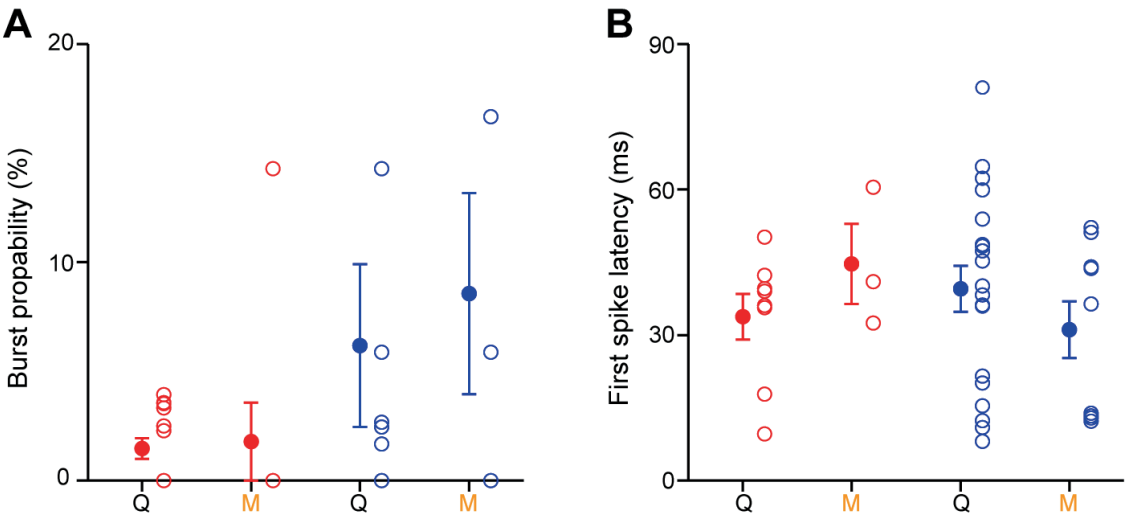

Figure 13. Temporal feature of supra-threshold activity evoked by sensory stimuli.
(A) The probability of burst firing in L2/3 and L5 neurons during sensory evoked PSP during both quiet wakefulness and movement.
(B) The first AP latency in sensory evoked PSP.

dedicated to the D3 of the forepaw. Brief and gentle tactile stimuli (2ms, 10mN) were delivered to the glabrous side of digit 3 via stimuli from the sensor arm. The stimulations followed a psuedo randomised pattern of delivery. V_m in both L2/3 and L5 exhibited an evoked postsynaptic potential (PSP) following a sensory stimulus in resting mice (Figure 12 A–C), and a transient increase in firing rates (Figure 12 D). Following a stimulus, the mean latency of first AP is quite similar for both layers, regardless of the cortical states (Figure 13). The subthreshold activity, however, exhibited differences that were strongly dependent on the state. During quietness, tactile stimulation could evoked a large subthreshold depolarization response in both L2/3 and L5 neurons, whereas the amplitude of tactile evoked response was reduced during digit movement in both layers (Figure12 C, E. $L2/3_{Amp}$ Q = 10.80 ± 0.65 mV, M = 4.84 ± 1.24 mV, n = 10 cells, P = 0.037; $L5_{Amp}$ Q = 6.19 ± 0.69 mV, M = 2.41 ± 0.60 mV, n = 20 cells, P = 0.001; Q $L2/3_{Amp}$ vs. $L5_{Amp}$ P < 0.001, M $L2/3_{Amp}$ vs. $L5_{Amp}$ P = 0.005). The amplitudes

of PSPs in L2/3 were larger than those in L5 (Figure 12 E), which might be due to the V_m baseline is more hyperpolarized in L2/3 pyramidal neurons. However, the mean evoked AP rates did not change much in either conditions, when the baseline AP rates were subtracted, it was shown that tactile stimulation did not evoked more APs in both layers, in both behavior states (Figure 12 F. $L2/3_{AP}$ Q = 1.59 ± 0.62 Hz, M = 1.95 ± 1.36 Hz, n = 10 cells, P = 0.375; $L5_{AP}$ Q = 2.44 ± 1.40 Hz, M = 1.55 ± 1.16 Hz, n = 20 cells, P = 0.370; Q $L2/3_{AP}$ vs. $L5_{AP}$ P = 0.613, M $L2/3_{AP}$ vs. $L5_{AP}$ P = 0.523).

To understand why the evoked AP rates showed only a moderate increase following tactile stimulation, in spite of the fact that the V_m was more depolarized, we first plotted the sensory responses as a function of the pre-stimuli onset V_m. As the V_m became more depolarized, the amplitude of sensory responses tended to fall until they reached negative levels (Figure 14). The point at which the amplitude was 0 mV was termed the sensory reversal potential. Sensory reversal potentials related to tactile stimuli were similar in periods of quietness and movement (Figure 12 G. $L2/3_{Rev}$ Q =-46.67 ± 1.60 mV, M =-47.09 ± 1.59 mV, n = 10 cells, P = 0.492; $L5_{Rev}$ Q =-46.17 ± 0.75 mV, M =-46.61 ± 0.86 mV, n = 20 cells, P = 0.412; Q $L2/3_{Rev}$ vs. $L5_{Rev}$ P = 0.644, M $L2/3_{Rev}$ vs. $L5_{Rev}$ P = 0.775). The closer the baseline V_m prior to stimulus onset is to the reversal potential, the smaller the PSP amplitude, and the reversal potentials in both layers are more hyperpolarized than the AP threshold (Mean: L2/3 $Q_{thr.}$=–36.89 mV, $M_{thr.}$=–35.25 mV; L5 $Q_{thr.}$=–36.75 mV, $M_{thr.}$=–37.16 mV). It lowers the probability of passing the AP threshold when the V_m of PSP reaches the reversal potential. It is worth

noticing that in a minority of cells which exhibit a smaller difference in V_m between the AP threshold and reversal potential, the AP rates are higher

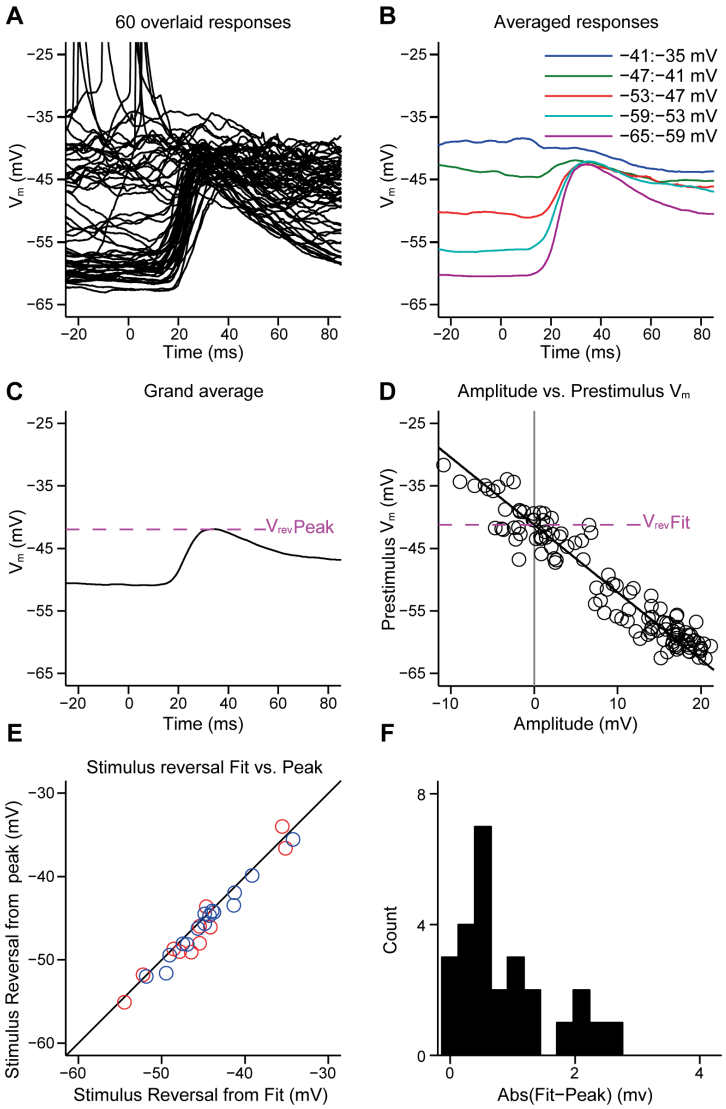

Figure 14. Measurement of the tactile-evoked sensory response reversal potential.
(A) Example trials of tactile evoked responses of a L2/3 cortical neuron in an awake mouse.
(B) Averaged tactile-evoked responses from neuron in (A) sorted into 5 categories based on the pre-stimulus V_m.
(C) Grand average from the example neuron in (A), pink dashed line shows the peak V_m of the grand average response (V_{rev}Peak).
(D) Plot of the amplitude of all individual tactile-evoked responses (open circles) from example neuron in (A) against the pre stimulus V_m. Pink dashed line shows the reversal potential as defined by the point at which the linear fit (black line) crosses the tactile-stimulus evoked response amplitude is 0mV(grey line).
(E) The peak V_m of the average tactile-evoked response (as in C) plotted against the reversal potential as determined by fitting the individual responses (as in D) shows significant correlation across all recorded cells. Red circles show L2/3 cells and blue circles L5 cells.
(F) Distribution of the differences in reversal potential as measured by both methods. The mean distance was 1 ± 0.15 mV.

(Figure 12 H). This means that the relatively hyperpolarized tactile reversal potential determines the ceiling of AP rates in tactile responses.

A similar state-dependent modulation manner of tactile responses in both L2/3 and L5 cells suggested a correlation in amplitude across cortical layers. We plotted the amplitude of responses under both conditions from trial to trial, obtaining a liner fitting across all responses which exhibited a highly correlated relationship between L2/3 and L5 in periods of both quiet wakefulness and movement (Figure 12 J,K). Another interesting trend appeared in our analysis of tactile responses from a dual recording (Figure 12 J). The distributions of amplitude are more diffused during quietness than during movement, which could be a result of a decrease in V_m variances during movement (Figure 2 D). Furthermore, we observed a correlation not only in the amplitude, but also in the onset latency of the response. The mean latencies for PSP and the first AP were similar in both L2/3 and L5 cells (Figure 12 I, $L2/3_{PSPLat}$ = 11.07 ± 0.58 ms, n = 13 v.s $L5_{PSPLat}$ = 11.34 ± 0.76 ms, n = 21, P = 0.972; Figure 13 B, $L2/3_{1stAPLat}$, Q = 33.78 ± 4.73 ms, n = 8 cells, M = 44.67 ± 8.30 ms, n = 3 cells; $L5_{1stAPLat}$, Q = 39.52 ± 4.72 ms, n = 19 cells, M = 31.10 ± 5.90 ms, n = 9 cells).

These data revealed a distinct character of the cortical sensory responses of L2/3 and L5 neurons in awake animals. Unlike the situation in the onset of slow frequency events, the sensory responses were highly correlated in amplitude and the onset of latency, which suggested that synchrony of sensory input might be a critical feature of cortical sensory processing.

3.1.8 L5 reports tactile stimuli related movement

During quietness, the mouse forepaw did not respond to tactile stimuli in most trials (75.2%). But on a few occasions (24.8%), the forepaw digit "fidgeted" after stimuli with a short latency (≦ 200 ms). When we analyzed sensory responses during quietness, we distinguished these two types of responses based on digit behaviour following tactile stimulation (Figure 15 A). Type I QM (Quiet–Move) was featured as a brief movement from the digit which closely followed PSP. In Type II, QQ (Quiet–Quiet), the digit remained stationary without a detectable displacement (Figure 15 A). Tactile stimulation evoked a large subthreshold response in both layers. The amplitude of sub-threshold PSPs were enhanced in QM responses in both layers (Figure 15 B, D. L2/3 QQ = 10.80 ± 0.65 mV vs. QM = 11.83 ± 0.79 mV, n = 10 cells, P = 0.037; L5 QQ = 6.19 ± 0.69 mV vs. QM = 8.16 ± 0.78 mV, n = 20 cells, P = 0.002; QQ L2/3 vs. L5 P< 0.001, QM L2/3 vs. L5 P = 0.005). In L5 neurons, QM responses were evoked at a more hyperpolarized pre-stimuli V_m than that of QQ responses (Figure 15 B, E. L2/3 QQ = –57.37 ± 1.36 mV, QM = –58.19 ± 1.58 mV, n = 10 cells, P = 0.232; L5 QQ = –52.53 ± 0.69 mV, QM = –54.24 ± 0.61 mV, n = 20 cells, P = 0.009; QQ L2/3 vs. L5 P = 0.006, QM L2/3 vs. L5 P = 0.033). This rendered them a stronger driving force during PSP to compensate for the hyperpolarized baseline V_m. After peak responses, the V_m of QQ briefly exhibited hyperpolarization, then depolarized to pre-stimuli levels with peaks at about 350 ms in both layers. In QM responses, a broader and even greater depolarization occurred following peak responses,

mimicking a brain state change (Figure 15 F. L2/3$_{post}$V$_m$ QQ = –57.18 ± 1.29 mV, QM = –53.55 ± 1.62 mV, n = 10 cells, P = 0.019; L5$_{post}$V$_m$ QQ = –51.89 ± 0.64 mV, QM = – 48.31 ± 0.8 mV, n = 20 cells, P < 0.001; QQ L2/3$_{post}$V$_m$ vs.

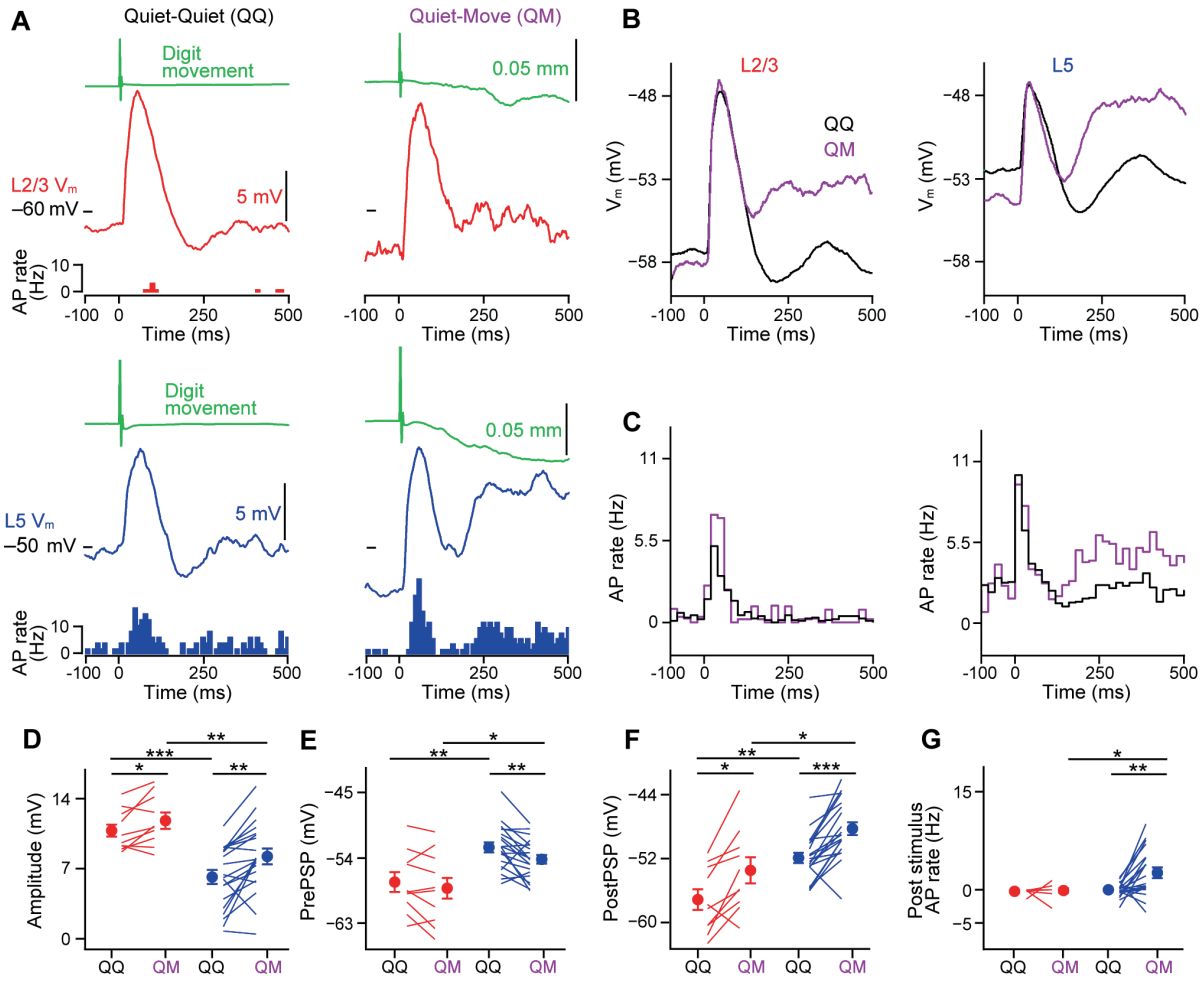

Figure 15. L5 neurons report tactile-stimuli related forepaw movements.
(A) Mean tactile triggered sensory postsynaptic potential(PSP)(V$_m$), with digit movement(green) and AP rates from a L2/3(red) and L5(blue) neuron. Right column stimuli triggered forepaw a fidget (QM), left column forepaw kept quiet after stimuli(QQ).
(B) Grand averaged tactile stimuli triggered sensory PSP from all recorded cells. Subthreshold V$_m$ of L2/3 and L5 cells for QQ and QM response, both L2/3 and L5 exhibit large depolarization phase following PSP;
(C) Grand AP rates PSTH in L2/3 and L5 neurons following tactile stimulation in QQ and QM trials. L5 neurons show suprathreshold response in the later phase (300-400 ms after stimulus onset).
(D) The amplitude of tactile-triggered subthreshold responses is significantly larger for QM trials than in QQ trials in both L2/3 and L5 neurons.
(E) The mean V$_m$ before stimuli(100 ms) is more hyperpolarized in QM trials than QQ trials in L5, but not in L2/3 neurons.
(F) The mean V$_m$ in the late phase(300–400 ms post stimuli onset) show grand depolarization in a QM trial in both layers.
(G) AP rates in late phase (background subtracted) are enhanced in QM trials in L5 neurons.
Filled circles with error bars show mean ± SEM. * P<0.05; ** P<0.01; *** P<0.001; L2/3 n=10; L5 n=20

$L5_{post}V_m$ P = 0.004, QM $L2/3_{post}V_m$ vs. $L5_{post}V_m$ P = 0.01). In addition, L5 neurons exhibited a drastic increase in AP rates during post-response depolarization, but nothing changed in L2/3 neurons (Figure 15 G. $L2/3_{post}$AP QQ =–0.18 ± 0.13 Hz, QM =-0.12 ± 0.34 Hz, n = 10 cells, P = 0.910; $L5_{post}$AP QQ =–0.01 ± 0.24 Hz, QM = 2.66 ± 0.81 Hz, n = 20 cells, P = 0.003; QQ $L2/3_{post}$AP vs.$L5_{post}$AP P = 0.613, QM $L2/3_{post}$AP vs. $L5_{post}$AP P = 0.011). This indicated that L5 was receiving extra excitatory inputs and/or was subject to less inhibition after stimulation. This feature suggests that L5 neurons are the best candidates as the reporters of sensory perception.

These data suggest that when stimulations are delivered during quiet wakefulness, L2/3 neurons exhibit larger amplitude of subthreshold responses, but L5 neurons elicit extra reporter spikes for movements that are generated in response to the stimulus. These results suggest an asynchronous output across cortical layers after sensory evoked PSP. In awake animals, our data for cortical sensory responses support L5 as the main source of output for sensory perception.

3.2 Cooling responses in SI L2/3

Sensory afferents in mice forepaw do not merely detect tactile sensory input, they are also responsible for thermal-sensory detection. This is typically the function of the transient receptor potential melastatin 8 (Trpm 8) channel in sensations related to an experience of mild cooling(Bautista et al., 2007). To test whether single cells in the primary somatosensory cortex (SI) respond to both mild-cooling and tactile stimulation, and if so, to characterize the cortical

responses, we set up a stimulation system for head-restrained mice under isoflurane anesthetization to enable one forepaw to receive both tactile and mild-cooling stimulations.

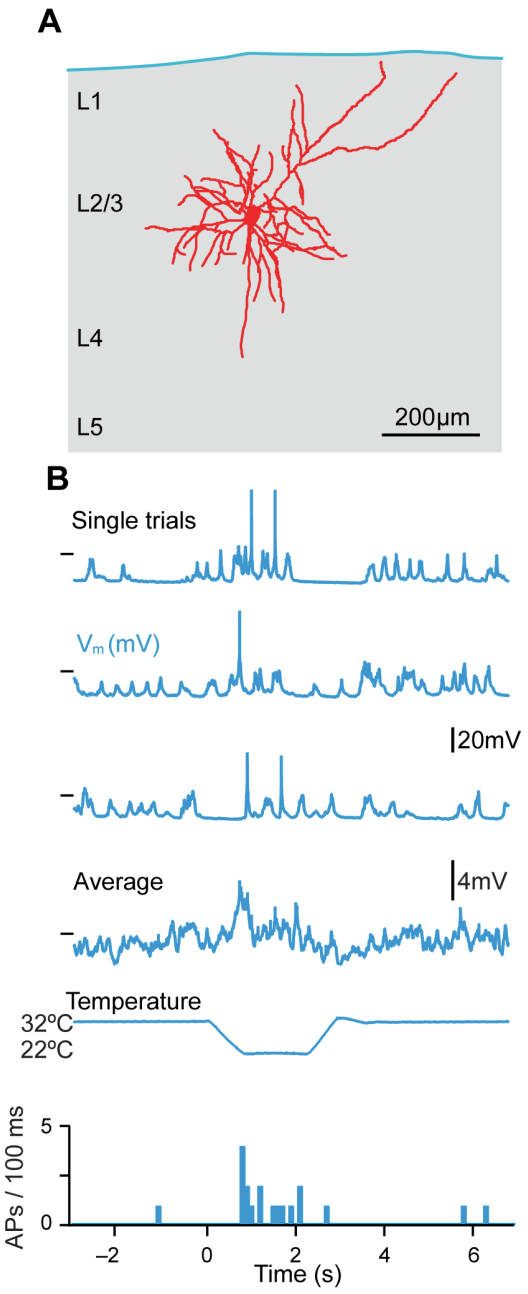

Figure 16. A L2/3 excitatory cortical pyramidal neuron in mouse forepaw SI respond to mild cooling stimuli.
(A)Biocytin staining reconstruction of a L2/3 pyramidal neuron in mouse forepaw SI. (B)Examples of the evoked response to mild cooling stimulation of the forepaw. Under example: mean membrane potential response and PSTH from 40 trials of cooling stimuli. Horizontal marks on V_m represent –60 mV for single trials and –74 mV for the mean response.

To assess whether mouse SI is involved in the perception of mild cooling (Figure 16), we targeted neurons in L2/3 to measure the cortical activity during cooling and tactile stimulation. Cooling stimuli (32-22℃) were

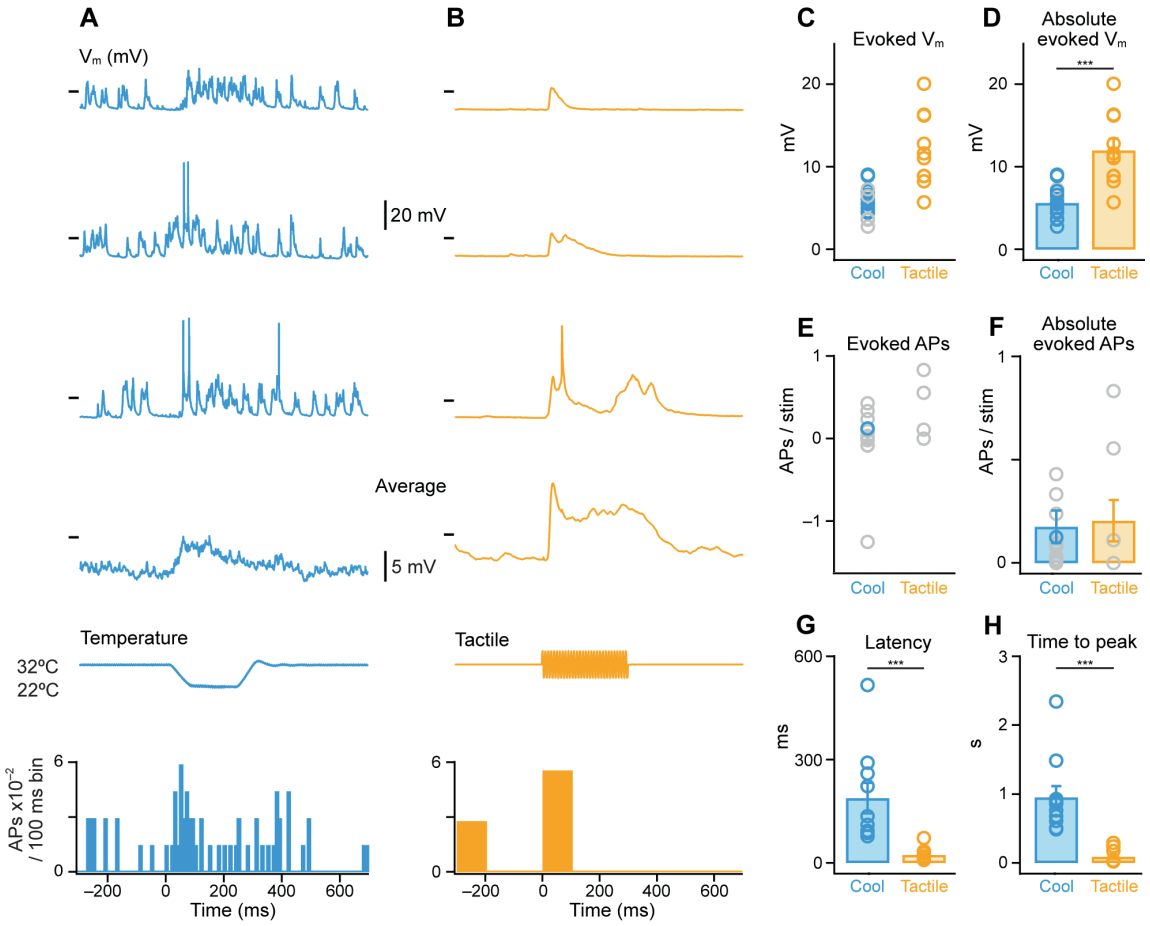

Figure 17. Evoked sensory responses from L2/3 neurons during cooling and tactile stimulation of the forepaw.
(A,B) Example of single trial sensory responses from the same cell to cooling (32–22 °C, blue, A) and vibrotactile (100 Hz, orange, B) stimulation of the forepaw at different time scales with averaged membrane potential responses and peri-stimulus time histograms (PSTH) shown below. Horizontal marks represent −60 mV.
(C) Evoked subthreshold sensory responses to mild cooling and tactile stimuli(cool, n = 16 cells from 11 mice; tactile, n = 10 cells from 8 mice).
(D) Absolute evoked peak sensory responses to mild cooling and tactile stimulation of the forepaw (cool, n = 16 cells from 11 mice; tactile, n = 10 cells from 8 mice).
(E) Evoked action potentials to mild cooling and tactile stimulation of forepaw(cool, n = 16 cells from 11 mice; tactile, n = 10 cells from 8 mice).
(F) Absolute evoked action potentials showed no significant difference between mild cooling and tactile stimulation (cool, n = 16 cells from 11 mice; tactile, n = 10 cells from 8 mice).
(G,H) Subthreshold sensory responses to mild cooling had a longer latency (cool, n = 10 cells from 8 mice; tactile, n = 10 cells from 8 mice) (G) and later time to peak (cool, n = 11 cells from 9 mice; tactile, n = 10 cells from 9 mice) (H) than during tactile stimulation.
Bars indicate mean population and error bars represent SEM. Gray points are non-significant responses.

presented to the forepaw digits 2-4 at 0.1 Hz or 0.05 Hz followed by a 100-Hz, 300 ms vibrotactile stimulus (Figure 17 A and B). The cooling of the forepaw evoked a sub-threshold response in 11 of 16 neurons with a range of 3.7–9.0 mV, and the tactile stimulus triggered a sub-threshold response as well in all neurons with a range of 5.7–20.1 mV. A comparison of absolute evoked membrane potential responses revealed a larger amplitude (amp.) for tactile (tac.) than cooling (cool) stimuli (Figure 17D, $Tac._{amp.}$=12.0 ± 1.4 mV; $Cool_{amp.}$=5.64 ± 0.46 mV, P=0.0001). However, neither cooling nor tactile stimulation evoked absolute changes in firing rates (AP) (Figure 17 F, $Cool_{AP}$= 0.18 ± 0.08 APs per stimulus, n = 16 neurons; Tac_{AP}=0.21 ± 0.10 APs per stimulus, n = 10 neurons; P = 0.4957). In a next step, we compared the kinetics of the sensory responses. The onset of the tactile stimulus-evoked responses were faster than that triggered by cooling as the latency(lat.) was shorter for the tactile stimulus (Figure 17G, $Tac_{lat.}$= 23.6 ± 5.9 ms, n = 10 neurons; $Cool_{lat.}$= 188.7 ± 44.1 ms, n = 10 neurons; P < 0.0001). The time needed to reach the peak was shorter for tactile stimuli as well (Figure 17 H, Tactile, 91.4 ± 32.5 ms, n = 10 neurons; Cooling, 953.8 ± 161.7 ms, n = 11 neurons; P < 0.0001). These data indicate distinct input circuits at the peripheral nerve endings, as tactile stimuli were conducted by thick myelinated sensory fibers such as Aα and Aβ, and cooling by thin fibers such as Aδ and C. The experiments confirmed that the L2/3 for the SI forepaw integrates multimodal sensory inputs such as tactile and cooling.

In mouse, which types of sensory receptors are responsible for mild-cooling stimulus? The transient receptor potential melastatin 8 (TRPM8)

expressed in sensory nerve terminals has been identified to mediate mild cool sensory transduction, as shown in mouse cold-avoidance behavior (Bautista et al., 2007). To test whether TRPM8 is involved in cortical cooling responses for the data shown above, we made *in vivo* recordings in SI forepaw of anesthetized mice with same stimulation protocol (Figure 18), in both TRPM8 KO and Wild-type (WT) littermates. These recordings revealed that 6 out of 8 WT mice showed a sub-threshold response to cooling. In

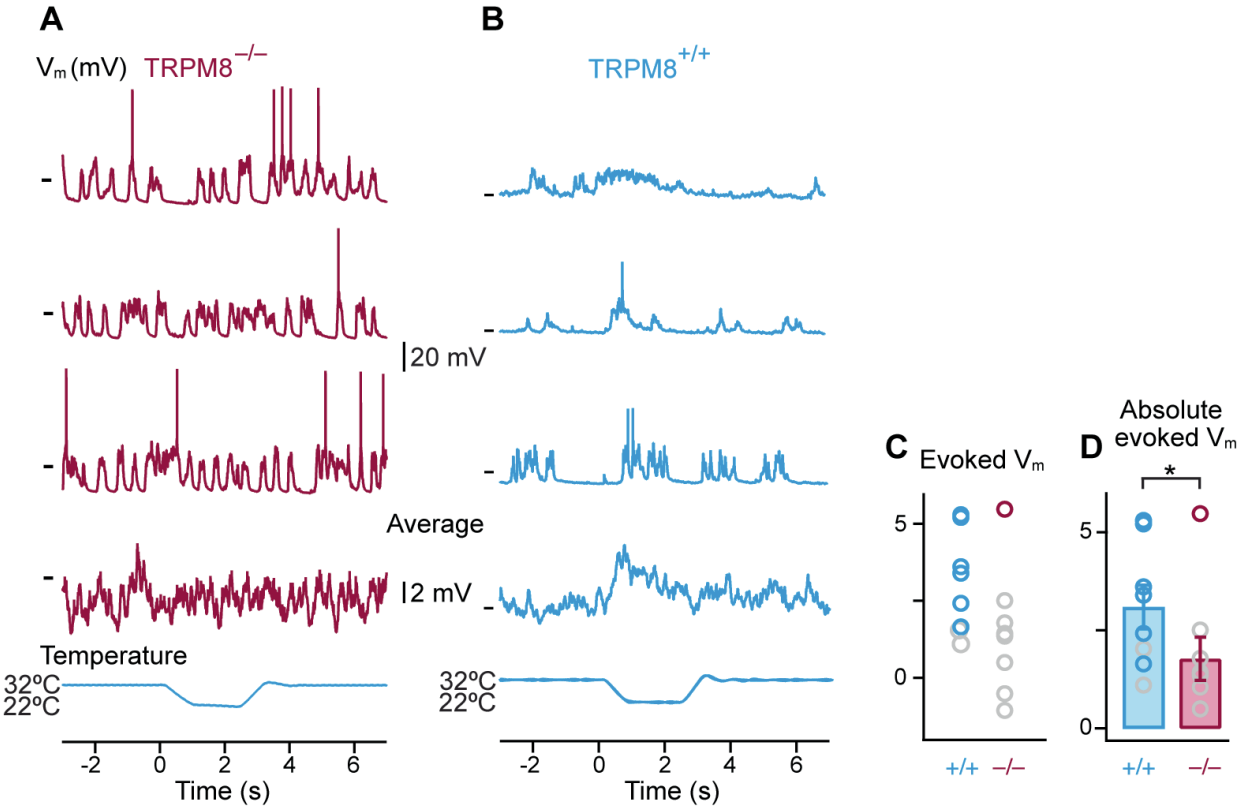

Figure 18. L2/3 neurons in *Trpm8*$^{-/-}$ mice do not respond to mild cooling stimulation of the forepaw
(A,B) Whole-cell recordings from L2/3 cortical neurons in a *Trpm8*$^{-/-}$ (a, magenta) and a *Trpm8*$^{+/+}$ (b, cyan) littermate control mouse showing single trials (above) and averaged response (below) to mild cooling stimulation. Horizontal marks on V_m represent −60 mV for *Trpm8*$^{-/-}$ and −50 mV for *Trpm8*$^{+/+}$.
(C) Evoked sensory responses to cooling. Each open circle shows an individual cell, significant responses are shown in colored circles and non-significant responses are shown in gray circles(n = 8 cells from 7 *Trpm8*$^{+/+}$ mice, 9 cells from 9 *Trpm8*$^{-/-}$ mice).
(D) Population absolute evoked sensory response exhibited that L2/3 neurons in forepaw SI of *Trpm8*$^{+/+}$ mice showed a larger subthreshold response to mild cooling than those of *Trpm8*$^{-/-}$ mice (n = 8 cells from 7 *Trpm8*$^{+/+}$ mice, 9 cells from 9 *Trpm8*$^{-/-}$ mice; P = 0.033).

TRPM8 KO mice, only 1 in 9 neurons (one out of 9 animals) exhibited responses to cooling. The amplitude of cooling responses was much larger in WT mice than in TRPM8 KO mice (Figure 18 d, Amp_{WT}= 3.09 ± 0.56 mV, n = 8 neurons; Amp_{KO}= 1.78 ± 0.51 mV, n = 9 neurons; P = 0.0333). However, the tactile response was not affected in TRPM8 KO mice (Figure 19). These data suggest TRPM8 conducts mild cooling sensations in mice, but their response kinetics were slower than those to tactile-evoked stimuli, due to the fact that different primary afferent fibers were activated by these two types of sensations. Together with behavioral data from another part of study from our lab (Milenkovic et al., 2014), we conclude that the forepaw SI is essential for mild cooling-induced perception.

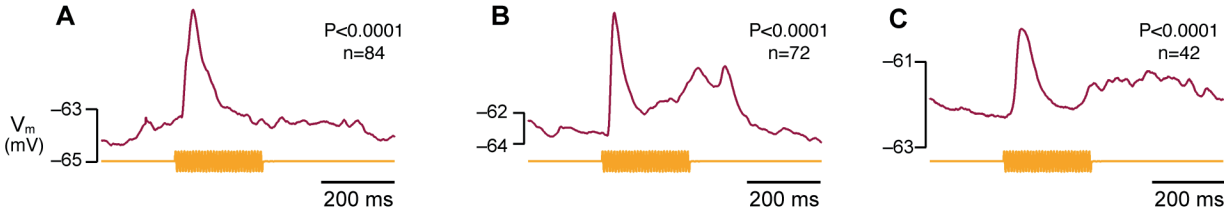

Figure 19. Layer 2/3 cortical neurons in *Trpm8*$^{-/-}$*mice* respond to tactile stimulation of the forepaw.
A, B, C, Three example cells from different mice showing significant averaged subthreshold responses (magenta) to 100 Hz vibrotactile stimulation (orange) of the forepaw digits.

4 Concluding remarks and discussion

Conclusion

This thesis examined the basic electrophysiological properties, spontaneous activity and sensory stimulation-evoked activities in L2/3 and L5 excitatory neurons in the forepaw primary somatosensory cortex (SI) of awake mice using in vivo whole-cell recordings combined with behaviour monitoring and tactile stimulation.

Our data revealed a layer-specific pattern of intracellular activities in SI that can be summarized as follows:

1) Excitatory neurons in L2/3 and L5 have specific cellular membrane properties, in particular L5 neurons are more excitable, more depolarized, show prominent after-hyperpolarization following current injection and have a larger input resistance.
2) Both layers show state dependent changes in subthreshold membrane potential dynamics, with slow frequency fluctuations abolished and replaced by higher frequency, smaller amplitude events, but L5 neurons firing more action potentials during movement.
3) The synchrony of subthreshold activity across layers 2/3 and 5 is dependent on the origin of the input: at the onset of forepaw movement and sensory responses, the SI exhibit a synchronous state across cortical layers whereas at the onset of slow frequency events and spontaneous action potential synaptic input has distinct timing.

4) Supra-threshold action potential firing (output) shows layer-specific responses following the onset of voluntary behaviour and sensory reception induced behavior with enhanced suprathreshold activity in L5.

All three observations raise a number of questions and suggest several avenues for future studies, which I will discuss below.

4.1 Excitation of L2/3 and L5 neurons

The intrinsic membrane properties and synaptic composition of L2/3 and L5 neurons have been studied in vitro from many cortical regions (van Brederode and Spain, 1995; Lefort et al., 2009; Petreanu et al., 2009; Perin et al., 2011; DeNardo et al., 2015). Previous reports have illustrated differences in the ion channel composition and density of excitatory and inhibitory neurons between L2/3 and L5 excitatory neurons (van Brederode and Spain, 1995; Lőrincz et al., 2002; Meyer et al., 2011). These features contribute to the basic excitatory membrane behaviour presented in our *in vivo* data. Compared to L2/3 excitatory cells, L5 receive more direct excitatory inputs from the thalamus and less inhibitory input from cortical circuits (DeNardo et al., 2015), which might makes its V_m more depolarized, thus more closed to AP threshold. Combining with higher input resistance, all these features support that L5 pyramidal neurons exhibits a higher level of excitation than those of L2/3 in spontaneous activity.

In addition, there is a high expression level of the ion channel/ conductance "I_h" channels in L5 excitatory neurons, which are absent in neurons of L2/3 (Lőrincz et al., 2002). This I_h channels could generate a

strong AHP at the offset of current injection and may underlying our observation of a prominent AHP in awake mice in L5 neurons. Presumably this AHP could help L5 neurons return to a baseline membrane potential after a period of intense spiking, and this would maintain a balance of membrane potential depolarization/hyperpolarization. I_h also regulates the formation of dendritic spikes during periods of long depolarizing inputs to L5 neurons (Larkum et al., 2009; Harnett et al., 2015), which is thought to be an efficient and robust form of information transfer.

4.2 Spontaneous cortical activity/brain states

Canonically, mammalian cerebral cortices are described as consisting of columns, and it has been suggested that primary somatosensory and visual cortices are also organized in functional columns whereas sensory input enters the cortex in a columnar fashion. However, many studies also show that cortical sensory processing and patterns of spontaneous activity involves the communication between different regions and may be more “column-free” than previous thought (Rakic & Caviness Jr, 1995; Horton & Adams, 2005; Poulet & Petersen, 2008; Polack et al., 2013; Zagha et al., 2013; Guy et al., 2015; Wagener et al., 2016). EEG recordings, which reflect global cortical activities are highly correlated with intracellular V_m or LFP across many cortical regions during wakeful quietness and anesthesia (Sheroziya & Timofeev, 2014). This suggests cortical slow frequency fluctuations are highly correlated in general, and do not confine within any kind of local structure. Moreover, LFPs exhibit highly correlated behavior across cortical regions in

broad temporal scale as well (Crochet et al.,). These data indicated that spontaneous fluctuations are not restricted within column boundaries, as exhibited by slow-frequency fluctuations. More and more evidence will be gathered to support the idea that spontaneous slow frequency fluctuations are globally distributed activities which are not confined within any specified “column”. Furthermore, in cerebral cortices, although thalamic projection to SI exhibit a barrel pattern (there are exceptions as primary visual and auditory cortices do not show barrel pattern), cortical activities(e.g slow frequency fluctuations) do not necessarily operate within single-column units, they might come across with thalamic input, but then spread out very quickly; an alternative is that they are organized as networks that are interleaved among columns. One might suppose that a central "processing unit" assigns functions to specific columns. Cortical columns might be more likely structural units rather than truly functional ones.

Although spontaneous slow frequency fluctuations are not restricted within specific cortical boundaries, they have layer-specific features in many cortical regions, as seen in data from both anesthetized and awake animals, and in vitro (Sanchez-Vives & McCormick, 2000; Sakata & Harris, 2009; Chauvette et al., 2010; Zhao et al., 2016). Previous membrane potential studies in neighbor L2/3 neurons has shown a highly cross correlation in wakeful quietness mice (Poulet & Petersen, 2008), which is caused by slow fluctuations. Our data show that neurons across cortical layers share the quite same degree of cross correlation in same behavior sate. Further more, close inspection of peak time of cross correlation, we find a time lag of about

9 ms (Figure 3). This suggests a characteristic that slow frequency fluctuations, or upstates (in the anesthetized brain) are generated earlier in deeper layers than in supra-granular layer as I showed in the results (Figure 5 and 7).

What could account for the timing difference between the SEFs onsets ? It could result from 1) higher proportion of inhibition in L2/3, which keep the hyperpolarized phase of slow frequency fluctuations in L2/3 relatively longer, 2) low firing rates of L2/3 pyramidal neurons, 3) layer-specific wiring pattern. As it was shown that L2/3 receive more long-range input from distant L2/3 neurons than L5 neurons. This suggests that activities in upper layers might be relative more independent on those occurring in deeper layers than previously thought. It might be a possible reason that intracellular and whole cell recording data report an earlier onset in upper layers in a portion of trials (Chauvette et al., 2010; Zhao et al., 2016). Another interpretation of earlier onset in L5 would be that more excitatory inputs from the thalamus and a high expression of I_h channels, which could help neurons recover from hyperpolarization sooner than those neurons that do not express this ion channel, such as L2/3 neurons. Besides, such latency differences would be the results of population activity, as shown in LFP and extracellular multiunit recordings, which is building up with spontaneous, but synchronous and or accumulated excitatory inputs, rather than initiated in a subset of L5 cells by spontaneous input alone.

Transitions in behaviour state in mice are typically accompanied by changes of cortical state. These changes exhibit layer-specific characteristics. In SI of the forepaw, as the behaviour state makes a transition from quietness to movement, subthreshold activity makes a synchronous transition to a sustained depolarization state. This could be due to synchronous excitatory inputs from both the thalamus (Poulet et al., 2012; Urbain et al., 2015) and the motor cortex (Zagha et al., 2013; Mao et al., 2011). The contrast between the sharp increase of firing rates was elicited in L5 neurons, while the firing rates in L2/3 did not change at all during the entire process suggest that L2/3 neurons may be strongly inhibited (Gentet et al., 2010). This layer-specific suprathreshold activity during the onset of movement suggests a weak role for L2/3 neurons in the transition of behavior state, and a key role for L5 neurons as the reporters of state transitions.

Many recent studies have indicated a depolarization of V_m ~100 ms before the onset of locomotion or pupil dilation as a reflection of changes in the dynamics of active internal attention (Polack et al., 2013; Schneider et al., 2014; McGinley et al., 2015). However, our data show a slight difference , as our grand averaged V_m starts to depolarize exactly when forepaw digits start to move, but with occasional observations of V_m depolarization prior to movement on a trial-to-trial basis. Such differences might be caused by criteria used to determine the onset of movement. Because in prior locomotion studies, animal movement was detected by tracking the velocity of wheel movement. We were able to detect movement on an order of μm/s, whereas other published data were only about 5–100 cm/s (Polack et al.,

2013; Schneider et al., 2014; McGinley et al., 2015; Vinck et al., 2015). The enormous difference in the degree of detection might have caused other groups to measure a longer latency in the onset of movement in reference to the incredibly fast V_m dynamics, which would appear as a change in neural activity prior to the onset of movement. Therefore, it is very likely that, V_m across SI cortical layers are synchronous with spontaneous movement onset. Or it could be that different types of movements have different motivations, some are reactive and others are planned , averaging the movements onsets would smear these together. Therefore in the future it will be important to measure the activity at movement onsets with a similar motivation in training behaving mice. Pupil diameter tracking might be another good method to monitor brain state changes as a complementary control for locomotion tracking.

4.3 Modulation of sensory processing in layers 2/3 and 5

In awake animals, sensory information undergoes active processing in the brain (Crochet et al., 2011). The response amplitude of each sensory stimulus is largely dependent on the ongoing brain states and membrane potential levels prior to the stimulus but differences exist between cortical regions. In the mouse VI, arousal and locomotion (active brain state) enhance visual responses (Bennett et al., 2013; Niell & Stryker, 2010; Polack et al., 2013; Reimer et al., 2014; Vinck et al., 2015), whereas in the whisker and forepaw barrel cortices (SI) and primary auditory cortex (AI), larger sensory responses are triggered during slow frequency oscillations (Crochet

& Petersen, 2006; McGinley et al., 2015; Zhao et al., 2016). While during movement, there is a reduction in subthreshold responses in both L2/3 and L5 of forepaw SI, as baseline V_m became more depolarized and close to reversal potential. Since the reversal potential of sensory responses is more hyperpolarized to AP threshold, therefore, there are not more APs were evoked by sensory stimulation. However, a few L5 neurons with higher sensory evoked AP rates, their reversal potentials are closer to AP threshold. It is likely that sensory stimulation also evoked a portion of local inhibition during behaviour, which might clamp the reversal potential of sensory responses below AP threshold in turn to regulating sensory coding.

Recent studies also showed that global spontaneous slow oscillations have the function of providing an optimal "nest" for sensory perception. The largest amplitude responses to sensory stimuli were those triggered during a more hyperpolarized phase of slow frequency oscillations than that of other sensory responses during quietness (McGinley et al., 2015; Zhao et al., 2016), which is called an “intermediate level of arousal” as shown by pupil diameter starting to increase to intermediate size (McGinley et al., 2015). This phenomenon could be interpreted as sensory stimulation evoked thalamic input enable to maximize its input effects while cortical network activities were crossing over its minimal level, given that spontaneous cortical activities are supposed to be noises while they are coming cross sensory input from thalamus. Besides, it is also indicated that the relationship between amplitude of subthreshold responses and behavior outcome is more

likely determined by pre-stimulation cortical states than the amplitude of stimulation.

In our data, most of the tactile stimuli triggered within this typical time window during quietness could induce 1) a fidgeting motion from forepaw digits, which were absent in the presence of other stimuli during the quiet period; 2) a broad and pronounced secondary depolarization after the decay phase of sensory evoked postsynaptic potentials in both L2/3 and L5 neurons; 3) the firing rates of L5 neurons were enhanced during secondary depolarization, it is a typical features of L5 which highlights its functions in reporting movement signals induced by feed-forward and feed-back of sensory evoked excitation. Therefore, future experiment could focus on the causal link of such sensory perception with behaviour outcome, whether it is a transformation of sensory input to motor output or prelude of active cortical state transition.

Although the amplitude and output of sensory evoked responses are modulated distinctly according to the behaviour states and the cortical states they encounter upon arrival, no overall difference was observed in the timing latency of sensory responses. Deep layers receive direct thalamic input (Meyer et al., 2010a, b; Constantinople & Bruno. 2014), which should support them register an earlier onset of sensory response, but L2/3 neurons are only one synaptic step away from L4 input. Moreover some VPM afferents directly terminate in L3, which would lead to activation of L3 within the same temporal window as L4 or L5. Such latency compensation in sensory processing is a significant advantage for animals' survival, as highly

synchronous cortical processing during sensory perception could minimize the reaction time needed to transform sensory signals into a behavioural outcome, and would win time for animals to escape from a threatening situation.

4.4 Cooling evoked sensory responses in SI

Besides respond to tactile stimulation, SI could also respond to mild cooling. Our data suggest that SI is directly involved in mild cooling sensation. It has been shown that TRPM8 receptor is responsible for mild cooling detection in peripheral sensory afferent. In our Trpm 8 KO mice, it is hardly to detect V_m responses in SI L2/3 neurons evoked by mild cooling, neither could they complete mild cooling detection task (Milenkovic et al., 2014), which was not impaired in wild type littermate control. It is also quite interesting that mild cooling and tactile stimulation could be detected in the same L2/3 neuron, which might enable the brain straightforwardly make an integrated perception about all the physical properties of an object.

In addition, we also find that the responses latencies of these two types of sensory response are quite different, as the latency of tactile response is much faster that that of mild cooling. It could be result of the velocity of sensory signal conduction is slower in fibers transducing cooling sensory signal, as these fibers are unmyelinated and thinner than those of transducing tactile sensory signal (Vallbo & Johansson, 1984; Johnson, 2001; Campero et al., 2001; Bautista et al., 2007; Schepers & Ringkamp, 2009).

4.5 Future direction

For the future, a number of behavioral tasks could be designed to more carefully dissect the functions of L5 neurons in communication within cortical circuits. Firstly, it might be necessary to identified the source and mechanism of earlier onsets of SFEs in L5, and the possibly function of earlier onset in L5. Secondly, study cortical processing during task-based behaviour with thalamic silencing will help understand the role of spontaneous cortical activity in behaviour state transition. Thirdly, since L5 is a direct target of inputs from the thalamus, L5 neurons must receive inputs from multiple senses in the forepaw system: including thermal and tactile stimuli and pain. This suggests that the forepaw might make an ideal model to address the complex issue of multi-sensory detection and integration. Finally, since L5 is the main output source of SI, it will serve as a fascinating window to monitor the relationship between cortical and subcortical input , output and behavior.

References

Adesnik, H. & Scanziani, M. Lateral competition for cortical space by layer-specific horizontal circuits. Nature 464, 1155–1160. (2010)

Adrian ED & Matthews BC. The Berger Rhythm: Potential Changes From The Occipital Lobes In Man. Brain 57, 355-385 (1934)

Barth AL. & Poulet JFA. Experimental evidence for sparse firing in the neocortex. Trends in Neurosciences 36, 345-355. (2012)

Bautista DM, Siemens J, Glazer JM, Tsuruda PR, Basbaum AI, Stucky CL, Jordt SE, Julius D. The menthol receptor TRPM8 is the principal detector of environmental cold. Nature 448, 204-8. (2007)

Chmielowska J, Carvell GE & Simons DJ. Spatial organization of thalamocortical and corticothalamic projection systems in the rat SmI barrel cortex. J Comp Neurol. 285, 325–338. (1989)

Bennett, C., Arroyo, S., and Hestrin, S. Subthreshold Mechanisms Underlying State-Dependent Modulation of Visual Responses. Neuron 80, 350–357 (2013).

Campero, M., Serra, J., Bostock, H. & Ochoa, J.L. Slowly conducting afferents activated by innocuous low temperature in human skin. J. Physiol. (London) 535, 855–865. (2001)

Castro-Alamancos, M.A. Absence of rapid sensory adaptation in neocortex during information processing states. Neuron 41, 455–464. (2004)

Cases O et al. Lack of Barrels in the Somatosensory Cortex of Monoamine Oxidase A–Deficient Mice: Role of a Serotonin Excess during the Critical Period. Neuron 16 , 297–307. (1996)

Chauvette S, Volgushev M, Timofeev I. Origin of active states in local neocortical networks during slow sleep oscillation. Cereb Cortex 20, 2660–2674. (2010)

Constantinople CM & Bruno RM. Deep cortical layers are activated directly by thalamus. Science 340, 1591–1594. (2013)

Crochet S & Petersen CC. Correlating whisker behavior with membrane potential in barrel cortex of awake mice. Nature Neurosci. 9, 608–610. (2006)

Crochet S, Poulet JFA, Kremer Y, Petersen CCH. Synaptic mechanisms underlying sparse coding of active touch. Neuron 69,1160-1175. (2011)

Deschênes M, Veinante P, Zhang ZW. The organization of corticothalamic projections: reciprocity versus parity. Brain Res Brain Res Rev. 28, 286-308. (1998)

Douglas RJ, Martin KA, Neuronal circuits of the neocortex. Annual Review of Neuroscience 27, 419–451. (2004)

Feldmeyer, D. Excitatory neuronal connectivity in the barrel cortex. Front. Neuroanat. 6, 24. (2012)

Feldmeyer D, Brecht M, Helmchen F, Petersen CCH, Poulet JFA, Staiger JF, Luhmann HJ, Schwarz C. Barrel cortex function. Progress in Neurobiology 103, 3-27. (2013)

Ferster D and Jagadeesh B. EPSP-IPSP interactions in cat visual cortex studied with in vivo whole- cell patch recording. The Journal of Neuroscience 12, 1262-1274. (1992)

Gentet LJ, Avermann M, Matyas F, Staiger JF, Petersen CC. Membrane potential dynamics of GABAergic neurons in the barrel cortex of behaving mice. Neuron 65, 422–435. (2010)

Gong Y, Huang C, Li JZ, Grewe BF, Zhang Y, Eismann S, Schnitzer MJ. High-speed recording of neural spikes in awake mice and flies with a fluorescent voltage sensor. Science 350,1361-6. (2015)

Groh A, Meyer HS, Schmidt EF, Heintz N, Sakmann B, Krieger P. Cell-type specific properties of pyramidal neurons in neocortex underlying a layout that is modifiable depending on the cortical area. Cereb Cortex 20, 826-836. (2010)

Guy J, Wagener RJ, Möck M, Staiger JF. Persistence of Functional Sensory Maps in the Absence of Cortical Layers in the Somsatosensory Cortex of Reeler Mice. Cereb Cortex 25, 2517-28. (2015)

De Kock, C. P. J. and Sakmann, B. High frequency action potential bursts (≥ 100 Hz) in L2/3 and L5B thick tufted neurons in anaesthetized and awake rat primary somatosensory cortex. The Journal of Physiology 586, 3353–3364. (2008)

de Kock, C. P., and Sakmann, B. Spiking in primary somatosensory cortex during natural whisking in awake head-restrained rats is cell- type specific. Proc. Natl. Acad. Sci. U.S.A. 106, 16446–16450. (2009)

Haider B, Duque A, Hasenstaub AR, Yu Y, McCormick DA. Enhancement of visual responsiveness by spontaneous local network activity in vivo.J Neurophysiol. 97, 4186-202. (2007)

Harnett MT, Magee JC, Williams SR. Distribution and function of HCN channels in the apical dendritic tuft of neocortical pyramidal neurons.
J Neurosci. 35,1024-37. (2015)

Harris, K.D. & Mrsic-Flogel, T.D. Cortical connectivity and sensory coding. Nature 503, 51–58. (2013)

Hattox AM, Nelson SB. Layer V neurons in mouse cortex projecting to different targets have distinct physiological properties. J. Neurophysiol. 98, 3330–3340. (2007)

Helmstaedter M, de Kock CP, Feldmeyer D, Bruno RM, Sakmann B, Reconstruction of an average cortical column in silico. Brain Research Reviews 55, 193–203. (2007)

Helmstaedter M, Sakmann B, Feldmeyer D. Neuronal correlates of local, lateral, and translaminar inhibition with reference to cortical columns. Cereb Cortex 19, 926-37. (2009)

Hooks BM, Hires SA, Zhang YX, Huber D, Petreanu L, Svoboda K, Shepherd GM Laminar analysis of excitatory local circuits in vibrissal motor and sensory cortical areas. PLoS Biol. 9, e1000572 (2011)

Horton JC, Adams DL. The cortical column: a structure without a function.
Philos Trans R Soc Lond B Biol Sci. 360, 837-62. (2005)

Houweling A, Brecht M. Behavioural report of single neuron stimulation in somatosensory cortex. Nature 451: 65-68. (2008)

Jasper HH. Electroencephalography. In: Penfield W, Erickson TC, eds. Epilepsy and Cerebral Localization. Springfield, IL: Charles C Thomas, 380-454 (1941)

Johnson KO. The roles and functions of cutaneous mechanoreceptors. Current Opining in Neurobiology 11, 455–461.(2001)

Jouhanneau JS, Ferrarese L, Estebanez L, Audette NJ, Brecht M, Barth AL, Poulet JFA. Cortical fosGFP expression reveals broad receptive field excitatory neurons targeted by POm. Neuron 84, 1065–1078. (2014)

T Lee, U Kim. Descending Projections From the Dysgranular Zone of Rat Primary Somatosensory Cortex Processing Deep Somatic Input. Journal of Comparative Neurology 520,1021–1046. (2012)

Lefort, S., Tomm, C., Floyd Sarria, J. C., and Petersen, C. C. The excitatory neuronal network of the C2 barrel column in mouse primary somatosensory cortex. Neuron 61, 301–316. (2009)

Larkum ME, Nevian T, Sandler M, Polsky A, Schiller J. Synaptic integration in tuft dendrites of layer 5 pyramidal neurons: a new unifying principle. Science 325, 756 –760. (2009)

Lőrincz, A., Notomi, T., Tamas, G., Shigemoto, R. and Nusser, Z. Polarized and compartment-dependent distribution of the hyperpolarization-activated channel HCN1 in pyramidal cell dendrites. Nature Neurosci. 5,1185-1193. (2002)

Ohno S, Kuramoto E, Furuta T, Hioki H, Tanaka YR, Fujiyama F, et al.
A morphological analysis of thalamocortical axon fibers of rat posterior thalamic nuclei: a single neuron tracing study with viral vectors. Cereb Cortex 22, 2840–57. (2012)

Manita S, Suzuki T, Homma C, Matsumoto T, Odagawa M, Yamada K, Ota K, Matsubara C, Inutsuka A, Sato M, et al. Neuron 86, 1304–1316. (2015)

Murayama M, Pérez-Garci E, Nevian T, Bock T, Senn W, Larkum ME. Dendritic encoding of sensory stimuli controlled by deep cortical interneurons. Nature 457,1137-41. (2009)

Margrie TW, Brecht M, Sakmann B. In vivo, low-resistance, whole-cell recordings from neurons in the anaesthetized and awake mammalian brain Pflugers Arch. 444, 491–498. (2002)

Mease RA, Metz M, Groh A. Cortical Sensory Responses Are Enhanced by the Higher-Order Thalamus. Cell Rep. 14, 208-15. (2016)

McGinley MJ, David SV, McCormick DA. Cortical membrane potential signature of optimal states for sensory signal detection. Neuron 87, 179–192. (2015)

Wimmer VC, Bruno RM, de Kock CP, Kuner T, Sakmann B. Dimensions of a projection column and architecture of VPM- and POm-axons in rat vibrissal cortex. Cereb Cortex 20, 2265-2276. (2010a)

Meyer HS, Wimmer VC, Hemberger M, Bruno RM, de Kock CP, Frick A, Sakmann B, Helmstaedter M. Cell type-specific thalamic innervation in a column of rat vibrissal cortex. Cereb. Cortex 20, 2287–2303. (2010c)

Meyer HS, Wimmer VC, Oberlaender M, de Kock CP, Sakmann B, Helmstaedter M. Number and laminar distribution of neurons in a thalamo-cortical projection column of rat vibrissal cortex. Cereb. Cortex 20, 2277–2286. (2010b)

Meyer H.S, Schwarz D, Wimmer VC, Schmitt AC, Kerr JN, Sakmann B, Helmstaedter M. Inhibitory interneurons in a cortical column form hot zones of

inhibition in layers 2 and 5A. Proceedings of the National Academy of Sciences 108,16807-16812. (2011)

Milenkovic N, Zhao WJ, Walcher J, Albert T, Siemens J, Lewin GR, Poulet JFA. A somatosensory circuit for cooling perception in mice. Nature Neurosci. 17, 1560-1566. (2014)

Mountcastle VB. Modality and topographic properties of single neurons of cat's somatic sensory cortex. J Neurophysiol. 20, 408–34. (1957)

Mountcastle VB. The columnar organization of the neocortex. Brain 120, 701–22. (1997)

Niell CM, Stryker MP. Modulation of visual responses by behavioral state in mouse visual cortex. Neuron 65, 472–479. (2010)

O'Connor DH, Peron SP, Huber D, Svoboda K. Neural activity in barrel cortex underlying vibrissa-based object localization in mice. Neuron 67, 1048–1061. (2010)

Otazu GH, Tai LH, Yang Y, and Zador AM. Engaging in an auditory task suppresses responses in auditory cortex. Nat. Neuroscience 12, 646–654. (2009)

Petreanu L, Mao T, Sternson SM, Svoboda K. The sub- cellular organization of neocortical excitatory connections. Nature 457, 1142–1145. (2009)

Perin R, Berger T K, and Markram H. A synaptic organizing principle for cortical neuronal groups. Proc. Natl. Acad. Sci. U.S.A. 108, 5419–5424. (2011)

Petersen CC, Hahn TT, Mehta M, Grinvald A, Sakmann B. Interaction of sensory responses with spontaneous depolarization in layer 2/3 barrel cortex. Proc Natl Acad Sci U S A. 100,13638-43. (2003)

Petersen CCH. Cell-type specific function of GABAergic neurons in layers 2 and 3 of mouse barrel cortex. Curr Opin Neurobiol. 26, 1-6. (2014)

Pidoux M, Mahon S, Deniau JM, Charpier S. Integration and propagation of somatosensory responses in the corticostriatal pathway: an intracellular study in vivo. J Physiol. (London) 589, 263-281. (2011)

Ramo´n y Cajal S. Textura del sistema nervioso del hombre y de los vertebrados. Imprenta N. Moya, Madrid (1904)

Rakic P, Caviness VS Jr. Cortical development: view from neurological mutants two decades later. Neuron 14, 1101-4. (1995)

Polack PO, Friedman J, and Golshani P. Cellular mechanisms of brain state–dependent gain modulation in visual cortex. Nature Neurosci. 16, 1331–1339. (2013)

Poulet JFA & Petersen CC. Internal brain state regulates membrane potential synchrony in barrel cortex of behaving mice. Nature 454, 881–885. (2008)

Poulet JFA, Fernandez LM, Crochet S, Petersen CCH. Thalamic control of cortical states. Nature Neurosci. 15, 370-372. (2012)

Reimer J, Froudarakis E, Cadwell CR, Yatsenko D, Denfield GH, Tolias AS. Pupil fluctuations track fast switching of cortical states during quiet wakefulness. Neuron 84, 355–362. (2014)

Sachdev RN, Ebner FF, Wilson CJ. Effect of subthreshold up and down states on the whisker-evoked response in somatosensory cortex. J Neurophysiol. 92, 3511-21.(2004)

Sakata S. & Harris KD. Laminar structure of spontaneous and sensory-evoked population activity in auditory cortex. Neuron 64, 404–418. (2009)

Sanchez-Vives MV, McCormick DA. Cellular and network mechanisms of rhythmic recurrent activity in neocortex. Nature Neurosci. 3,1027–1034 (2000)

Schepers RJ & Ringkamp M. Thermoreceptors and thermosensitive afferents. Neurosci. Biobehav. Rev. 33, 205–212. (2009).

Schneider DM, Nelson A, Mooney R. A synaptic and circuit basis for corollary discharge in the auditory cortex. Nature 513, 189–194. (2014)

Sheroziya M, Timofeev I. Global intracellular slow-wave dynamics of the thalamocortical system. J Neurosci. 25, 8875-93. (2014)

Shepherd GM, Stepanyants A, Bureau I, Chklovskii D, Svoboda K. Geometric and functional organization of cortical circuits. Nature Neurosci. 8, 782-90. (2005)

Silberberg G, Markram H. Disynaptic inhibition between neocortical pyramidal cells mediated by Martinotti cells. Neuron 53, 735-46. (2007)

Steriade M & McCarley RW. Brainstem Control Of Wakefulness And Sleep (Plenum Press, New York, 2005).

M Steriade, I Timofeev, F Grenier. Natural waking and sleep states: a view from inside neocortical neurons J. Neurophysiol. 85, 1969–1985 (2001)

Urbain N, Salin PA, Libourel PA, Comte JC, Gentet LJ, Petersen CC. Whisking-Related Changes in Neuronal Firing and Membrane Potential Dynamics in the Somatosensory Thalamus of Awake Mice. Cell Reports 13, 647–656 (2015)

Vallbo AB, Johansson RS. Properties of cutaneous mechanoreceptors in the human hand related to touch sensation. Hum Neurobiology 3, 3-14. (1984)

van Brederode J.F., Spain W.J.. Differences in inhibitory synaptic input between layer II-III and layer V neurons of the cat neocortex. J. Neurophysiol. 74, 1149–1166 (1995)

Vinck M, Batista-Brito R, Knoblich U, Cardin JA. Arousal and locomotion make distinct contributions to cortical activity patterns and visual encoding. Neuron 86, 740–754. (2015)

Wagener RJ, Witte M, Guy J, Mingo-Moreno N, Kügler S, Staiger JF. Thalamocortical Connections Drive Intracortical Activation of Functional Columns in the Mislaminated Reeler Somatosensory Cortex. Cereb Cortex 26, 820-37. (2016)

Wiesel TN, Hubel DH. Ordered arrangement of orientation columns in monkeys lacking visual experience. J Comp Neurol. 158, 307–18. (1974)

Wimmer VC, Bruno RM, de Kock CP, Kuner T, Sakmann B. Dimensions of a projection column and architecture of VPM and POm axons in rat vibrissal cortex. Cereb Cortex 20, 2265-76. (2010)

Wise SP & Jones EG. Cells of origin and terminal distribution of descending projections of the rat somatic sensory cortex. J Comp Neurol. 175, 129–157. (1977)

Woolsey TA & Van der Loos H. The structural organization of layer IV in the somatosensory region (SI) of mouse cerebral cortex. The description of a cortical field composed of discrete cytoarchitectonic units. Brain Res. 17, 205–242. (1970)

Tan AYY, Chen Y, Scholl B, Seidemann E, Priebe N J. Sensory stimulation shifts visual cortex from synchronous to asynchronous states. Nature 509, 226–229 (2015)

Zagha E, Casale AE, Sachdev RN, McGinley MJ, and McCormick DA. Motor cortex feedback influences sensory processing by modulating network state. Neuron 79, 567–578. (2013)

Zhao WJ, Kremkow J, Poulet JF. Translaminar Cortical Membrane Potential Synchrony in Behaving Mice. Cell Rep. 15, 2387-2399. (2016)

Zhou M, Liang F, Xiong XR, Li L, Li H, Xiao Z, Tao HW, and Zhang LI. Scaling down of balanced excitation and inhibition by active behavioral states in auditory cortex. Nature Neurosci. 17, 841–850. (2014)

Acknowledgments

There are many people to whom I would like to express my appreciation, for their help and supports.

Firstly, I would like to thank my current and former supervisors: James Poulet, Wang Zhongfeng and Yang Xiong-Li. They open the door of neural science to me. With their great help I acquired a solid technology of patch clamp recordings. Furthermore, they also provide significant advices and instruction on my way of pursuing academic career.

Secondly, I would like to thank my colleagues, they help me quite a lot in many ways. Jens Kremkow contributed a lot of analysis in my PhD project, Janett König provided a lot help in biocytin staining and other things, Evgeny Bobrov for proofreading our paper and my dissertation, Nevena Milenkovic-Zujko shared her project with me, Jean-Sebastien Jouhanneau shared the lab room and conference hotel with me. In addition, I would like to thank graduate and welcome office in MDC, they make my stay in Berlin convenient, Russell Hodge for proofreading my thesis. And the institute of neuroscience in Shanghai, I enjoyed the talks and symposiums there when I was a freshmen of neuroscience.

Finally, I want to thank my friends and family. I have a lot of fun with these friends during my PhD, and some of them let me know more about Classic music and violin. I would like to express my heartfelt appreciation to my deceased grandmother-in-law, she passed away during my PhD, and required not to tell me about her situation as she did not want to disturb my work. I feel deeply sorry and sad about that. She and my grandfather-in-law are very kind, nice and wise people who supported me to make and pursue my choice.

This thesis is dedicated to my grandparents-in-law and parents.

Publications

Zhao WJ, Kremkow J, Poulet JF. Translaminar Cortical Membrane Potential Synchrony in Behaving Mice. Cell Rep. 15, 2387-2399. (2016)

Milenkovic N, **Zhao WJ**, Walcher J, Albert T, Siemens J, Lewin G, Poulet J. A somatosensory circuit for cooling perception in mice. Nature Neuroscience 17, 1560-1566. (2014)

Declaration of independence

I hereby declare that this dissertation contains my own independent work and that I have not received help from other groups.

I did not use any other sources, figures or resources than the ones stated in the bibliography. This includes possible figures or tables.

I marked all passages and sentences in my work that were taken from other sources clearly as such and named the exact source. Furthermore I declare that – to my best knowledge – this dissertation has not been submitted by me or somebody else at this or any other universities.

I confirm that I have not committed plagiarism in the accomplishment of this dissertation, nor have I falsified and/or invented experimental data.

I accept the academic penalties that may be imposed for violations of the above.